NAVAL POSTGRADUATE SCHOOL

MONTEREY, CALIFORNIA

THESIS

SEA LEVEL VARIABILITY ANALYSIS FOR COASTAL NAVAL INSTALLATIONS

by

Monica L. Killoran

June 2022

Co-Advisors: Mara S. Orescanin
Scott Powell

THIS PAGE INTENTIONALLY LEFT BLANK

REPORT DOCUMENTATION PAGE			*Form Approved OMB No. 0704-0188*

1. AGENCY USE ONLY *(Leave blank)*	**2. REPORT DATE** June 2022	**3. REPORT TYPE AND DATES COVERED** Master's thesis

4. TITLE AND SUBTITLE
SEA LEVEL VARIABILITY ANALYSIS FOR COASTAL NAVAL INSTALLATIONS

5. FUNDING NUMBERS
RLQ51

6. AUTHOR(S) Monica L. Killoran

7. PERFORMING ORGANIZATION NAME(S) AND ADDRESS(ES)
Naval Postgraduate School
Monterey, CA 93943-5000

8. PERFORMING ORGANIZATION REPORT NUMBER

9. SPONSORING / MONITORING AGENCY NAME(S) AND ADDRESS(ES)
Naval Information Warfare Center Pacific, San Diego, California(CA) 92152

10. SPONSORING / MONITORING AGENCY REPORT NUMBER

11. SUPPLEMENTARY NOTES The views expressed in this thesis are those of the author and do not reflect the official policy or position of the Department of Defense or the U.S. Government.

12a. DISTRIBUTION / AVAILABILITY STATEMENT
Approved for public release. Distribution is unlimited.

12b. DISTRIBUTION CODE
A

13. ABSTRACT (maximum 200 words)

Extreme sea levels near the coast can cause severe risk to life and infrastructure, and while forecasts are improving, understanding and planning for these events remains a challenge. Sea level variability (SLV) is controlled by complex local and remote multiresolution forces that interact, excite, and evolve under the influence of climatic and non-climatic factors in the ocean and atmosphere. The magnitude and strength of connection between forcing allows for development of foundational environmental knowledge of processes influencing SLV. This study proposes a methodology that identifies the distinct spatial patterns of SLV at small scale and depicts sea-level response to atmospheric teleconnection parents. A normalized characterization process of SLV was developed and tested by using technology resources and information already available. Verification of the methodology using a proof-of-concept region, San Diego Bay, revealed that it is possible to characterize processes that are unique to each location. Additional findings suggest that an analysis of high-resolution altimetry contrasted with local measures allows for identification of distinct spatial patterns of water levels at coastal and deep-ocean regions with representation of SLV response to climatic-driven processes on a global scale. This methodology was formulated such that it can be used at other locations globally as a tool to better quantify the risks of extreme water levels.

14. SUBJECT TERMS climate variability modes, coastal water levels, sea level variability, information warfare, meteorology, oceanography, remote sensing, geographic information systems, climate change	**15. NUMBER OF PAGES** 105
	16. PRICE CODE

17. SECURITY CLASSIFICATION OF REPORT	**18. SECURITY CLASSIFICATION OF THIS PAGE**	**19. SECURITY CLASSIFICATION OF ABSTRACT**	**20. LIMITATION OF ABSTRACT**
Unclassified	Unclassified	Unclassified	UU

NSN 7540-01-280-5500

Standard Form 298 (Rev. 2-89)
Prescribed by ANSI Std. 239-18

THIS PAGE INTENTIONALLY LEFT BLANK

Approved for public release. Distribution is unlimited.

SEA LEVEL VARIABILITY ANALYSIS FOR COASTAL NAVAL INSTALLATIONS

Monica L. Killoran
Lieutenant Commander, United States Navy
BS, Francisco Jose de Caldas District University, 2003
MS, University of Maryland University College, 2013

Submitted in partial fulfillment of the
requirements for the degree of

MASTER OF SCIENCE IN METEOROLOGY AND PHYSICAL OCEANOGRAPHY

from the

NAVAL POSTGRADUATE SCHOOL
June 2022

Approved by: Mara S. Orescanin
Co-Advisor

Scott Powell
Co-Advisor

Peter C. Chu
Chair, Department of Oceanography

THIS PAGE INTENTIONALLY LEFT BLANK

ABSTRACT

Extreme sea levels near the coast can cause severe risk to life and infrastructure, and while forecasts are improving, understanding and planning for these events remains a challenge. Sea level variability (SLV) is controlled by complex local and remote multiresolution forces that interact, excite, and evolve under the influence of climatic and non-climatic factors in the ocean and atmosphere. The magnitude and strength of connection between forcing allows for development of foundational environmental knowledge of processes influencing SLV. This study proposes a methodology that identifies the distinct spatial patterns of SLV at small scale and depicts sea-level response to atmospheric teleconnection parents. A normalized characterization process of SLV was developed and tested by using technology resources and information already available. Verification of the methodology using a proof-of-concept region, San Diego Bay, revealed that it is possible to characterize processes that are unique to each location. Additional findings suggest that an analysis of high-resolution altimetry contrasted with local measures allows for identification of distinct spatial patterns of water levels at coastal and deep-ocean regions with representation of SLV response to climatic-driven processes on a global scale. This methodology was formulated such that it can be used at other locations globally as a tool to better quantify the risks of extreme water levels.

THIS PAGE INTENTIONALLY LEFT BLANK

TABLE OF CONTENTS

LIST OF FIGURES

LIST OF TABLES

THIS PAGE INTENTIONALLY LEFT BLANK

LIST OF ACRONYMS AND ABBREVIATIONS

AAO	Antarctic Oscillation
AO	Arctic Oscillation
CO-OPS	center for operational oceanographic products and services
CPC	NOAA climate prediction center
CPSD	cross power spectral density
DOD	Department of Defense
DON	Department of the Navy
ECU	environmental coastal units
ENSO	El Nino Southern Oscillation
EOFs	empirical orthogonal functions
EWL	extreme water level
GAO	Government Accountability Office
GIS	geographic information system
IA	inter-annual
m	meters
MEaSUREs	making Earth system data records for use in research environments
METOC	meteorology and oceanography
MJO	Madden–Julian Oscillation
mm	millimeters
MSL	mean sea level
NAO	North Atlantic Oscillation
NASA	National Aeronautics and Space Administration
NAVFAC	Naval Facilities Engineering Command
NCAR	National Center for Atmospheric Research
NOAA	National Oceanic and Atmospheric Administration
PDO	Pacific Decadal Oscillation
PNA	Pacific-North American oscillation
PSL	physical sciences laboratory
RQD	research quality data
S2A	intra-annual

S2S	sub-seasonal to seasonal write once read many
SA	solar annual tidal constituent
SLC	sea level change
SLP	sea level pressure
SLV	sea level variability
SOCAL	Southern California
SSA	solar semiannual tidal constituent
SSHA	sea surface height anomaly
SWL	still water level
USGS	United States Geological Survey
UTide	unified tidal analysis and prediction
VLM	vertical land motion
WMO	World Meteorological Organization

ACKNOWLEDGMENTS

My sincere appreciation to Dr. Mara Orescanin, Dr. Scott Powell, and their families for their continued support, mentorship, and encouragement throughout this interesting learning opportunity. The completion of this work would not been possible without the advice of Mr. Mike Cook, Dr. Mark Merrifield, Dr. Angelica Rodriguez and Dr. Leslie Bolick.

To the Green family, the Johnson family, the Nadaf family, and my cohort: I am grateful for the support provided throughout our time at NPS.

THIS PAGE INTENTIONALLY LEFT BLANK

I. MOTIVATION

The Navy operational mission is primarily supported by coastal installations located within latitudes of 48N and 8S and in towns that have considerably large populations, industries, and robust transportation systems. Naval facilities are vulnerable to Sea Level Change (SLC) and the impacts from sea level variability (SLV) tend to be more significant during extreme water level events. SLV is caused by combinations of forcing factors that occur at different spatial and temporal scales, varying from short term, sub seasonal events to seasonal, interannual and multidecadal climate variations. The impacts of changing sea levels include coastal flooding, inundation, and damage of infrastructure. The enhanced global warming producing changes in weather patterns combined with regional and local sea level variability lead to a significant risk to naval logistic support.

The Department of Defense (DOD) and Department of the Navy (DON) priorities on Climate in the areas of national security, operational sustainment, planning, and readiness, align with scientific quests of understanding Earth's Sea variability as a direct result of changing climate (DOD 2021; Del Toro 2021). Providing a solution that addresses differences of global, regional, and local sea level patterns can provide effective means to present and integrate relevant environmental information to a Defense decision making process in support of facilities planning and management (Keogh and Törnqvist 2019).

Recent Government Accountability Office (GAO) reports on Climate Resilience and adaptation (GAO 2017, 2019) showed that there is a need for DOD standards on climate projections and its incorporation into installations' planning. The DOD has concurred with the findings and recommendations to ensure "identification of authoritative sources of such projections, use of projections involving multiple future scenarios, and what future time periods to consider" (GAO 2019). The DON with its versatile mission and forward presence faces an imminent challenge of adapting and providing logistical solutions in support of fleet operations. As DOD continues the work of "research and products that fuse climate science, design, and decision sciences methods in the context of current DOD/Service planning, operations, and management" (DOD 2019), understanding

tendencies in sea level, as well as the relationship between global, regional, and local sea level variability, provides key insights about the impacts of the Earth's climate on the ocean and atmosphere.

The Naval Facilities Engineering Command (NAVFAC) has developed a robust sea level and Flooding Geographic Information System (GIS) tool for managing of environment and installations that facilitates planning, readiness, and sustainment of operations using National Oceanic and Atmospheric Administration (NOAA) authoritative products. The solution accounts for climate impacts and has a special feature that includes SLC and Extreme Water Level (EWL) using a regional coastal sea level risk scenario study (Hall et al. 2016; Moss et al. 2016; Chadwick et al. 2013). Initial review of the report suggests there is a gap on data and standards for certain locations; the methods applied as well as some findings are in need for validation, update, or refinement. Globalization and technology advances hinder integration and interoperability across sectors leaving society with data overloads and a gap between science and policy.

The current transition to a new space era, the unprecedented evolvement of a pandemic and significant climate changes, drive the need for innovative long-term ways to sustain and support military operations. According to Han et al. (2019), "satellite altimetry data show unambiguous regional differences in sea level trends since the late 20th century"; therefore, understanding and predicting the environment in a standard manner is critical for mission success and logistic support sustainability. The focus of this study is to determine how sea level variability of coastal areas could be represented for any naval facility. If this approach proves to be accurate, this could allow the DOD to quickly examine multiple sea level contributing processes at coastal facilities and provide actionable science supported by data analytics to aid adaptation, mitigation, and resilience plans.

II. INTRODUCTION

A. BACKGROUND

SLV is driven by a multi-scale array of diverse local and remote processes that interact, excite, and evolve under the influence of climatic and non-climatic factors in the atmosphere and ocean. Although there are significant advances and lines of effort committed to sea level change, its underlying causes are not fully understood at local levels and this usually happens at coastal places owing to amplification or modification of open ocean processes. Processes in various nonlinearly coupled aspects of the planetary system fuel SLV, and understanding these processes is therefore a highly active topic of interdisciplinary research (Bindoff et al. 2007; Woodworth et al. 2019). The complexity of SLV lays in the different temporal and spatial scales of all processes involved, as well as the lack of understanding influences of each process relative to a location.

At global scales, SLV is mainly due to three processes: non-linear thermosteric variability as seawater thermal expansion, halosteric changes as ocean salinity variation, and barystatic variability as water mass contribution and exchange between oceans and other water reservoirs (Wang et al. 2017; Gregory et al. 2019; Palmer et al. 2020). Such processes are related to climate change via global warming and ocean warming, including anthropogenic influences, which combined with land mass composition and distribution cause geographically non-uniform variability.

At the regional and local scales, deviation from the global contribution is owing to a group of varying processes in time and space that impact coastal SLV: i) sterodynamic changes in ocean dynamics, ocean physics and climate modes; ii) short-term effects, i.e., variations influenced on periods shorter than weeks (such as synoptic weather patterns); iii) water masses such as glaciers, ice sheets, and land water storage; and iv) vertical Land Motion (VLM) such as subsidence, tectonics, gravitational pull, and glacial isostatic adjustment (GIA) that influence measurement of levels without alteration of water volume (Stammer et al. 2013; Beckley et al. 2017; Frederikse et al. 2020; Hamlington et al. 2020; Felikson et al. 2020). At local scales, boundary-imposed changes from the continental shelf

to the shoreline and the coastline excite extreme water levels and pose a risk for coastal flooding due to erosion, storms, precipitation, waves, water runoff, mean sea level, and tides (Bindoff et al. 2007; Oppenheimer et al. 2019). The relative role and importance of the local and remote driving forces in determining high and low frequency SLV is still inconclusive (Barnard et al. 2019; Benveniste et al. 2020; IPCC 2021).

Global and regional sea levels can be currently calculated using two types of observations: in-situ, mainly by irregularly spaced and spatially distributed tide gauges, and remotely sensed using satellite altimeters (Gangadharan et al. 2017; Safi'i & Rudiastuti 2019; Xu et al. 2019; Bahman et al. 2018; Benveniste et al. 2020; Hamlington et al. 2021). Tide gauges constitute the oldest method of data gathering and provides local sea level calculations relative to land with VLM dependencies. In contrast, altimetry is the most continuous method on a global scale that provides accurate geocentric sea level estimates around the world but with poor spatial and temporal resolution of coastline signals (Woodworth et al. 2017b; Han et al. 2019; Church et al. 2014) compared to in situ gauge datasets. Additional data from buoys and drifters provides details on processes such as steric sea levels and waves (Ezer 2013; Wang et al. 2017).

B. SLV CHARACTERIZATION

Past and ongoing research extensively investigate atmospheric and oceanic SLV forcing at coastlines and have found significant limitations to budget closings due to non-linear feedbacks and coupled dynamics such as the overview of time and space multi-scale processes contributing to coastal SLV described by Woodworth et al. (2019) and represented in Figure 1; acknowledging that there are still significant limitations on defining exact scales for each process, in this study, SLV will be best categorized into key processes by timescales.

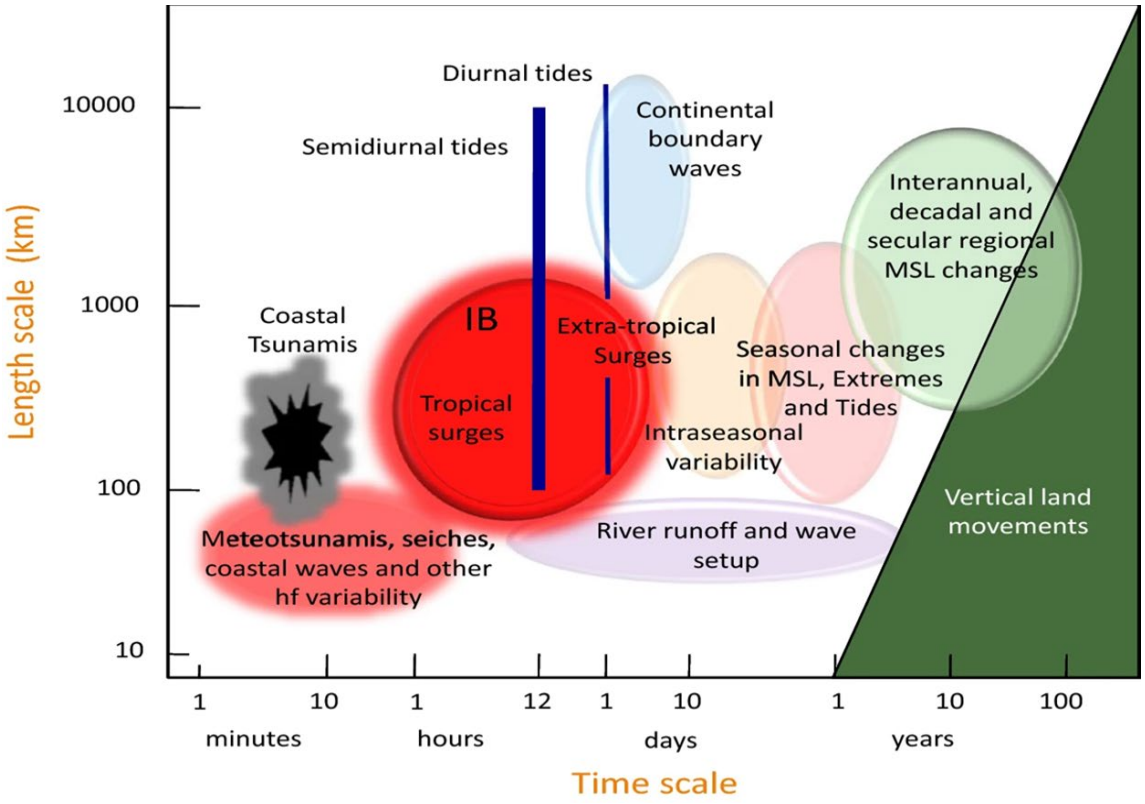

"A schematic overview of processes contributing to sea level variability at the coast indicating the space and timescales involved." Source: Woodworth et al. (2019).

Figure 1. Coastal Sea Level Variability Contributing Processes

1. Tides

Tidal fluctuations are the most dominant and well-understood oscillation in coastal SLV (Thompson et al. 2021); however, complexity is added by the planetary or orbital-derived tidal constituents and coastal generated tidal resonance (NASA 2000). In coastal shallow waters, adding gravitational pull of periodic orbital motions of Earth, the sun, and the moon, generate harmonics and over tides which comprise the 37 total constituents (Parker 2017), ranging from hours, days, seasons, to years (4.4- and 18.6-year cycles). Tides are linked to seiches, storm surge activities, seasonal effects, oceanic dynamics, and climate (Pugh and Woodworth 2014; Ray and Merrifield 2019; Habel et al. 2020).

2. Seasons

Seasonal signals are significant extratropical SLV drivers ranging from atmospheric mechanisms (precipitation, pressure, and winds), water mass exchange (ice melting, river run offs), ocean circulation (wind derived strength), to steric effects t(thermal and haline) (Felikson et al. 2020; Hamlington et al. 2021; Dangendorf et al. 2021).

3. Non-tidal Components

a. Transient Signals

High frequency signals, which are defined herein as having periods of less than 15 days, strongly influence SLV at the coast with a tendency to increase internal variability due to topography, bathymetry, dynamics, and resonance (Woodworth et al. 2019). Storm surges, wave runup (as swash and wave setup), seismic tsunamis, seiches, and coastal meteotsunamis (mainly from air pressure disturbances), can superimpose exacerbating EWL and accelerate the intensity and severity of coastal flooding events. (Stockdon et al. 2006; Menendez and Woodworth 2010; Merrifield et al. 2013; Idler et al. 2019; NOAA 2021).

b. Sub-seasonal to Seasonal (S2S)

This work defines S2S variability as that with periods between 15 and 115 days. Intraseasonal oscillations, mainly the Madden–Julian Oscillation (MJO) (Madden and Julian 1971, 1972; Zhang et al. 2005) and the Boreal Summer Intraseasonal Oscillation (Jiang and Wang 2004) have strong SLV effects in the tropics and subtropics with a large role on EWL events occurrence (Oliver and Thompson 2010; Klotzbach and Oliver 2015; Pajak and Kowalczyk 2018; Liu et al. 2021). S2S forcing in conjunction with locally dependent dynamics and mean sea level (MSL), are the bridge of atmospheric and oceanic interactions across spatial and temporal scales (Gill 1982; Pajak and Kowalczyk 2018; Payo-Payo and Bertin 2020; Long et al. 2021).

c. Low Frequency Signals

Low frequency signals are classified herein as having periods longer than 115 days and include intra-annual, inter-annual, and decadal oscillations. They consist mainly of

climate modes within the coupled ocean-atmosphere system that have been associated with coastal MSL variability (Han et al. 2017a; Han et al. 2019; Hermans et al. 2020; Xiaoyu et al. 2020; Xu et al. 2019; Zhu et al. 2021) and are described more in the next section.

C. CLIMATE VARIABILITY MODES

Influences from S2S, interannual and decadal variability presented as teleconnection patterns associated with the ocean circulation and coastal processes are valuable to understand the time-varying relationship between climate modes and SLV (Chafik et al. 2017; Leamon et al. 2021; Zhu et al. 2021). The phase and states of global and regional scale climate variables that are monitored by climate models are characterized by indices of recognized oscillations spreading over large areas across the world. For this research, 7 indices are identified for study that may be related to SLV.

1. Circulation Modes

There are four circulation indices (WMO 2021) widely used that are based upon empirical orthogonal functions (EOFs). The Arctic Oscillation (AO), also known as Northern Hemisphere Annular Mode (NAM) is characterized by symmetric, annular, non-seasonal anomalies of sea level pressure (SLP) affecting the polar vortex at middle to high northern latitudes with two phases (positive and negative) that impact SLV through sea surface temperature changes. Its phase periodicity extends from few days to two weeks, but its phase variability is random, lasting up to few months. The Antarctic Oscillation (AAO) or Southern Annular Mode, is the analogous mode of AO at the southern hemisphere defined by the westerly winds and low-pressure changes around Antarctica (Thompson and Wallace 2000). The North Atlantic Oscillation (NAO) is characterized by a positive and a negative phase of sea level pressure changes over the North Atlantic Ocean, driving the location of storm tracks and strength of westerly winds with intra-annual and inter-annual variability (NOAA CPC 2022). The Pacific-North American (PNA) oscillation is characterized by two phases of alternating pressure anomalies (Rossby wave pattern) between the central Pacific, western Canada and southeastern United States, driving the strength of the mid-latitude jet stream with very irregular low frequency variability. (NOAA CPC 2022).

2. El Nino Southern Oscillation (ENSO) And Pacific Decadal Oscillation (PDO)

ENSO is a large-scale oceanic-atmospheric interaction, associated with warming in the equatorial Pacific region causing precipitation, temperature, and winds disturbances, with intra-annual to inter-annual variability. ENSO indices are based on equatorial sea surface temperature anomalies calculated relative to a 30-year base period with the number of the index referring to SST regions with in 5° of the Equator; Niño 3.4, corresponds the 170° to 120° West region; and Niño 4, corresponds the 160° East to 150° West region (Trenberth and NCAR 2020). PDO, resembles an ENSO pattern with decadal variably in the northeast and tropical Pacific Ocean, characterized by warm or cool SST and SLP anomalies. A positive PDO value represents North Pacific below average SLP and cool SST in the interior with warm SST along the Pacific coast, and the opposite is true for a negative PDO value (Mantua 1999). The PDO index is calculated using an extended SST reconstruction.

3. MJO

A variability component of the Walker circulation, MJOs are complex S2S disturbances of the global ocean-atmospheric system such as rainfall, winds, pressure, and clouds, that usually start in the tropical Indian Pacific region and propagates eastward through the tropics with some equatorial Rossby and Kelvin waves patterns. It consists of eight phases characterized by either enhanced or suppressed rainfall traversing the globe in the tropics and returning to its origin in 30 to 60 days influencing temperature, tropical cyclone activity and precipitation patterns across the globe (Tseng et al. 2020). MJO indices are calculated using extended EOF (EEOF) of velocity potential anomalies equatorward of 30°N and projecting them into ten time-lagged patterns with the number of the index referring to a specific longitude canter of enhanced convection (NOAA CPC 2022).

Figure 2 depicts the generalized location of strongest manifestation of climate variability modes; however, their patterns largely vary in time and space.

Generalized location of strongest manifestation of main climate variability modes that characterize and explain spatial patterns of precipitation, pressure, and temperature are represented by name and color. Circulation modes AO, AAO, PNA and NAO (blue), ENSO (red), MJO (purple) and, PDO (dark gray). Image Source: Esri via ArcGIS Pro.

Figure 2. Atmospheric Teleconnections

Additional geographically dependent factors such as erosion, land motion, morphology, and anthropogenic forcing, are considered in the characterization of processes but their detailed analysis is beyond the scope of this study.

D. HYPOTHESIS AND RESEARCH QUESTIONS

Hundreds of naval facilities in coastal regions are vulnerable to changing sea levels and accurately measuring how much and how quickly sea level varies at specific timeframes is a complex scientific quest but critical to reducing risk at these installations. Recent advances in research have enabled the measurement and projection of SLC scenarios, but there are local (usually coastal) level details still missing that can help to determine how to proactively mitigate and adapt to sea level variability. The depiction of temporal changes has been studied (Church et al. 2013; Cazenave et al. 2017; Beckley et

al. 2017; Fox-Kemper et al. 2021); however, detailed measurement of non-tidal processes contributing to those changes at a given location is still needed (Ezer 2013; Hamlington et al. 2020). This research intends to develop foundational environmental knowledge of climate patterns influencing coastal SLV that better serve decision making processes for coastal naval installations than directly support ship operations.

The objectives of this study are as follows:

1) Determine the processes that influence SLV and can be captured and measured by both altimetry and tide gauges;

2) Distinguish the main climate and non-climate driven processes contributing to changes on sea level at selected coastal areas; and

3) Quantify contributions to variability for coastal naval installations via climatology SLV "thumbprints."

The hypothesis is that SLV components derived from altimetry and tide gauge data can provide information on key processes driving coastal water level variability and quantify relative magnitudes of these processes. To test the hypothesis, the research focuses on SLV at different spatial and temporal scales at selected locations that allow the development of a forcing methodology by comparing and analyzing high-resolution altimetry contrasted with in-situ measures and environmental conditions that allows identification of distinct spatial and temporal patterns and depiction of processes to determine how sea level responds to natural and anthropogenic forcing.

The operational goal of this study is to improve the Defense decision making process for coastal installations by integrating environmental information at relevant scales in a spatial analysis framework. The objectives are to account for meteorological and ocean forcing factors, show multitemporal patterns in SLV, and construct uniform and valid SLV approximations.

III. METHODS

To dissect the relative components of SLV at any specific location, tide gauge water level and altimetry sea surface height anomaly (SSHA) timeseries were contrasted with climate mode indices to determine sea level contributors, to discern climate-driven processes and, to quantify SLV aggregated contributions. The data and techniques used to examine SLV in the vicinity of San Diego, California are described in this chapter.

A. ALTIMETRY DATA, IN-SITU OBSERVATIONS, AND CLIMATE INDICES

Southern California (Figure 3) sea levels were selected as proof of concept as the locations provide offshore forcing characterization for enclosed basins (San Diego Station) and open beaches (La Jolla Station) as well as regional coastal patterns (SOCAL altimetry grid point). Additional sites and global analysis were analyzed to validate efficacy of the method.

Three types of datasets were used to conduct this research. The water level contribution analysis was sourced from hourly and daily Still Water Level (SWL) tide gauge Research Quality Data (RQD) using a/the standard station benchmark as the datum reference (Caldwell et al. 2015). Gauge data was analyzed from San Diego (station 9410170), located at 32° 42.9′ N, 117° 10.4′ W, and La Jolla (station 9410230), located a32° 52.0′ N, 117° 15.4′ W. The locations of both stations along the San Diego area coastline are illustrated in Figures 3c and 3d. The analysis period is from, from 02 October 1992 to 31 December 2019, encompassing available data during the satellite altimetry era.

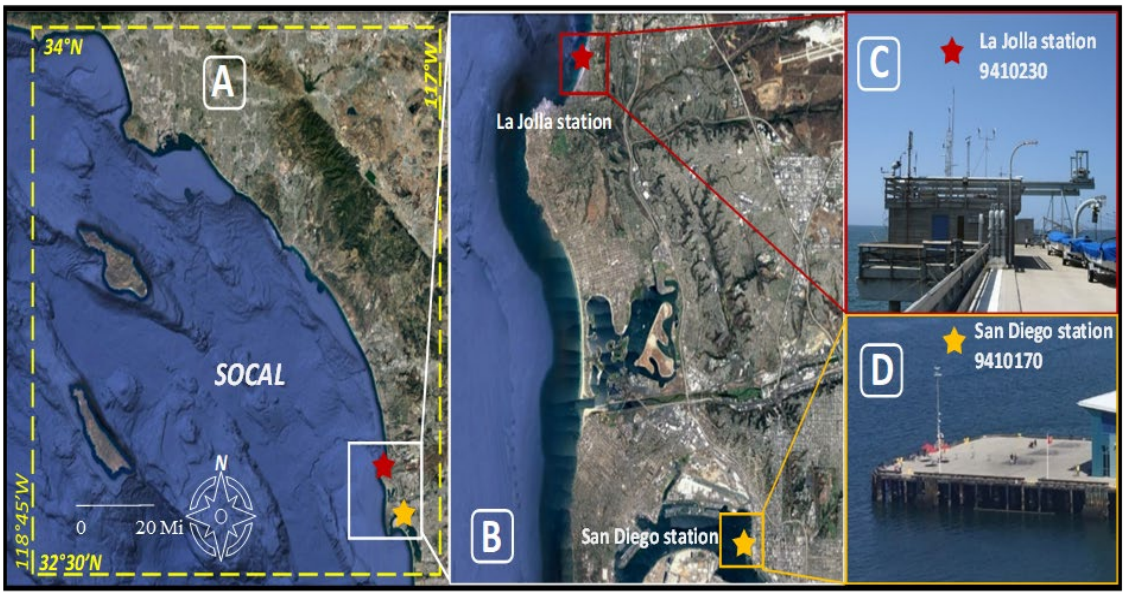

Data source locations relative to Southern California coastal region. A. Altimetry area of study (dashed yellow line); tide gauges location (white line). B. Zoomed in Location of La Jolla and San Diego still water level stations. C. Photograph of station 9410230, La Jolla, CA. D. C. Photograph of station 9410170, San Diego, CA. Images Source: Google Earth and NOAA.

Figure 3. Southern California Data Source Locations

While gauge data provide a long record of frequently recorded water levels, they may only be representative of SLV in a small area near the gauge location. Remote sensing of sea level from space provides a global characterization of SLV that gauge data alone cannot; however, the tradeoff is that the spatiotemporal resolution of space-borne data is relatively crude (10 miles every 120 hours). In this work, altimeter estimates of sea level anomalies were provided by the Making Earth System Data Records for Use in Research Environments (MEaSUREs) gridded Sea Surface Height Anomalies (SSHA) product, which is available at a temporal resolution of 5 days and spatial resolution of 0.17° by 0.17° from October 1992 to January 2019 (Zlotnicki 2019).

This work uses the altimeter data to first demonstrate consistency between it and gauge data San Diego and La Jolla as examples and second to expand analysis of SLV to the entire globe, including locations where tide gauge data may not be readily available. To minimize computations, the SSHA spatial analysis was degraded to 2.5° × 2.5° resolution with the native five-day time step of the MEaSUREs data product.

Statistical tests between sea water levels derived from both gauge and altimeter data and climate mode indices (Chapter IV.F) were completed using daily and monthly atmospheric and ocean climate indices (Table 1) from the NOAA Climate Prediction Center (CPC) and Physical Sciences Laboratory (PSL).

B. PARAMETERS, ASSUMPTIONS, LIMITATIONS, AND SCOPE

Sea level was the only parameter used to conduct the presented analysis. Datasets to which the method could be applied are assumed to be quality-controlled for research applications. Data gaps ware curated using the SWL station verified hourly water level archive for tide gauge timeseries or by interpolation for altimetry timeseries. The period of analysis was limited to availability of altimetry data (October 1992 to January 2019) climate mode indices (1981 to 2021). Although standard analysis was performed for a span of 26-years (October 1992 to December 2019), some additional calculations were completed for the periods of January 1981 to December 2019 (mainly to assess climate-driven SLV), and from October 1992 to January 2019 (for assessing SLV using SSHA). SWL measurements are relative to the sea level defined to the station tide staff zero, which is linked to land-based benchmarks and therefore are susceptible to VLM, a process that cannot be directly contrasted to altimetry data unless resolved by geodesic analysis. The present study is intended only to broadly depict SLV at surface and resolve for gaps between single point datasets at the coastline and coarse resolution regional grids. Time frames were defined as October 1992 to January 2019 for sea level assessments and from 1981 to present to assess potential relationships between SLV and the climate variability mode indices outlined in Chapter II.

Table 1. Climate Indices Contrasted to SLV

Geophysical system	Data Length	Index details
Teleconnections/ circulation	1950-Present	North Atlantic Oscillation (NAO) Arctic Oscillation (AO) Antarctic Oscillation (AAO) Pacific/North American Pattern (PNA)
Source: www.cpc.ncep.noaa.gov/products/precip/CWlink/daily_ao_index/teleconnections.shtml		
El Nino Southern Oscillation (ENSO)	1981 to Present	Niño 3 (5°North-5°South) (150°West-90°West) Niño 3.4 (5°North-5°South) (170-120°West) Niño 4 (5°North-5°South) (160°East-150°West)
Source: https://www.cpc.ncep.noaa.gov/data/indices/		
Madden-Julian Oscillation (MJO) Ten time-lagged patterns	1978 to Present	MJO 1 (80° East) MJO 2 (100° East) MJO 3 (120° East) MJO 4 (140° East) MJO 5 (160° East) MJO 6 (120° West) MJO 7 (40° West) MJO 8 (10° West) MJO 9 (20° East) MJO 10 (70° East)
Source: www.cpc.ncep.noaa.gov/products/precip/CWlink/daily_mjo_index/mjo_index.shtml		

Source: NOAA PSL, NOAA CPC, and World Meteorological Organization (WMO) Climate Explorer.https://climexp.knmi.nl/selectdailyindex.cgi?id=someone@somewhere

C. SEA LEVEL TIMESERIES ANALYSIS

1. Key Indicators

Considering the SLV forcing factors previously described, coastal SWL is defined as:

$$\eta_{SWL} = \eta_{Tide} + \eta_{Res} \qquad (1)$$

in which η_{SWL} is the sea level (η_a) measured at a tide gauge, η_{Tide} represents the tidal components of the SWL, and η_{Res} represents the residual non-tidal components of the SWL.

To calculate η_{Tide}, a harmonic analysis and tidal fit of the hourly SWL time series was preformed using Unified Tidal Analysis and Prediction (UTide) functions (Codiga 2022). To characterize sea level trends, the SWL, tidal fit and residual datasets were linearly detrended and sea level change was calculated for a 40-year period and a 26-year period, then contrasted to the NOAA sea level trend that encompasses all available water levels at each station. The same process was done for SSHA sea level (η_a), and comparison of results highlighted the rate at which sea level is changing at different periods of time.

Averaging of hourly SWL was used to estimate, validate, and remove the seasonal component of η_{SLW}, which is composed of the seasonal components of η_{Tide}, plus the seasonal component of η_{Res}, then contrasted to the annual (SA) and semiannual (SSA) tidal fits. For altimetry, an average of η_a was used to calculate seasons.

To classify and broadly assess key tidal and non-tidal SLV indicators, the largest 30 water levels were identified for η_{SLW}, η_{Tide}, and η_{Res}, and the largest 10 events were identified for η_a. This facilitated the identification of individual or combined SLV drivers within the timeseries and the contrast of largest events for all locations in the area.

2. Non-tidal Components

The non-tidal water level can be further split by periodicity as follows:

$$\eta_{Res} = \eta_{Tr} + \eta_{S2S} + \eta_{S2A} + \eta_{IA} + \eta_{DC} \qquad (2)$$

in which η_{Tr} is the transient phenomena that occur with periodicities less than 15 days such as storm-driven variability or wave setup. η_{S2S} is the sub seasonal to seasonal (S2S) phenomena that occur with periods between and 15–115 days (such as the MJO). η_{S2A} denotes intra-annual (S2A) phenomena with periods between 115 days and 1 year. η_{IA} represents inter-annual (IA) phenomena with periods of 1–10 years (such as ENSO). Finally, η_{DC} contains slowly varying decadal phenomena with periods greater than 10 years such as the PDO.

Fourier low and high pass filters were applied to the de-seasoned, de-trended η_{Res} (also referred as residual) to estimate transient, S2S, S2A, IA and decadal components. Cut-oof frequencies were based on η_{Tr}, η_{S2S}, η_{S2A}, η_{IA}, and η_{DC} periodicities.

3. SLV Contributors

To quantify contributions of SLV processes at coastal areas that are exclusive to each location, a climatology SLV "thumbprint" was developed stacking individual water level contributions at each timestamp. The output provides a unique "fishbone" like representation of all contributors and identifies events that were extreme in the timeseries, which is extremely valuable to interpret SLR scenarios. The 98th and 99th percentiles of η_{SLW}, η_{Tide}, η_{a}, and η_{Res} were identified to analyze exceedance of water levels and determine the impact of each non-tidal contribution.

4. Maximum Water Levels

Maximum values were estimated for each filter to determine the highest possible value of sea level at any given time of the year if all components were to constructively interfere with each other at the same time, producing a EWL representation of each location per month which is helpful to identify possible time of occurrence and type process contributing to severe SLV.

5. Climate-Driven SLV

To determine the main climate-driven processes contributing to SLV, initial monthly climate mode indices correlation to MEaSUREs monthly time series from NASA Data Analysis Tool (DAT) 2.0 from NOAA CPC was completed to select most relevant modes to include in the analysis. Daily and monthly climate indices were useful in highlighting atmospheric impacts and effects on SLV. Correlation coefficients and kappa coefficients were calculated for each daily filtered water level with respect to the daily climate modes presented in Table 1. PDO index was omitted in the daily analysis as it only is reconstructed monthly.

Pearson correlation coefficients (ρ), magnitude squared coherence and cross power spectral density (CPSD) were calculated to implement a signal spectral analysis (Welch

1967). To evaluate the strength of connections between signals by reducing the spectral coherence to a scalar value, a κ coefficient calculation method was adapted to determine the ocean response of sea level to individual contributors or to the climate variability modes following Oliver and Thompson (2010); results were used to validate Chapters IV and V analysis, and a visualization is available in the Appendix. Correlation and coherence-squared were used, as they tell different relationship aspects; coherence identifies if there is a relationship by looking at frequency space similarities for two variables, so it is useful for determining whether sea water level is somehow related to a climate mode. Correlations tells the direction of that relationship by calculating the extent to which two variables covary, which is particularly useful for cyclical indices like MJO1–10.

Bootstrapping was applied for estimating significance level for the cross-spectra coherences between water level and climate mode time series (Kaplan 2004; Shumway and Stoffer 2000). Autocorrelation was not accounted for in the time series, which if properly done, would reduce the degrees of freedom available for estimating statistically significant ρ or κ.

THIS PAGE INTENTIONALLY LEFT BLANK

IV. SAN DIEGO SEA LEVEL TIMESERIES ANALYSIS

A. ENVIRONMENTAL CHARACTERISTICS

The area of study defined in Figure 2 is described under the United States Geological Survey (USGS) Environmental Coastal Units (ECU) as ECU 2 and ECU 6. San Diego station is in an enclosed basin bounded by the man-made silver strand and exposed to the bay phenomena (such as seiches); La Jolla station falls under the protected oceanside littoral cell with narrow shelf and controlled man-made intervention, resembling characteristics of a natural beach.

ECU 2 is characterized as flat or sloping or steeply sloping with 60.9% average slope, sinuous, non-erodibility, warm temperate dry, moderate river discharge, moderate wave energy with average significant wave height of 0.88 meters (m) and average turbidity of 0.22(m^{-1}), moderately tidal with average tidal range of 2.37 m, euhaline-oxic-warm to very warm, clear, and low chlorophyll, in the vicinity of San Diego and La Jolla tide gauges. The SOCAL area is also under ECU 6: sloping or steeply sloping with 49.95% average slope, straight, high erodibility, warm temperate dry, moderate river discharge, moderate wave energy with average significant wave height of 1.02 m and average turbidity of 0.36 m^{-1}, moderately tidal with average tidal range of 1.98m, euhaline-oxic-moderate to cool, clear, and low chlorophyll.

B. KEY INDICATORS

Hourly detrended SWL data for San Diego, California is shown in Figure 4. Figure 4a depicts SWL timeseries with the 30 largest events for SWL (gray vertical lines), tides (white vertical dashed lines) and residual (black vertical dotted lines). Figure 4b depicts the tidal fit timeseries with the 30 largest tidal events highlighted in white dash lines. Figure 4c depicts the residual timeseries with the 30 largest tidal events highlighted in dotted black lines. In each panel, the highest and lowest values of the timeseries, and the dates on which they occurred, are denoted.

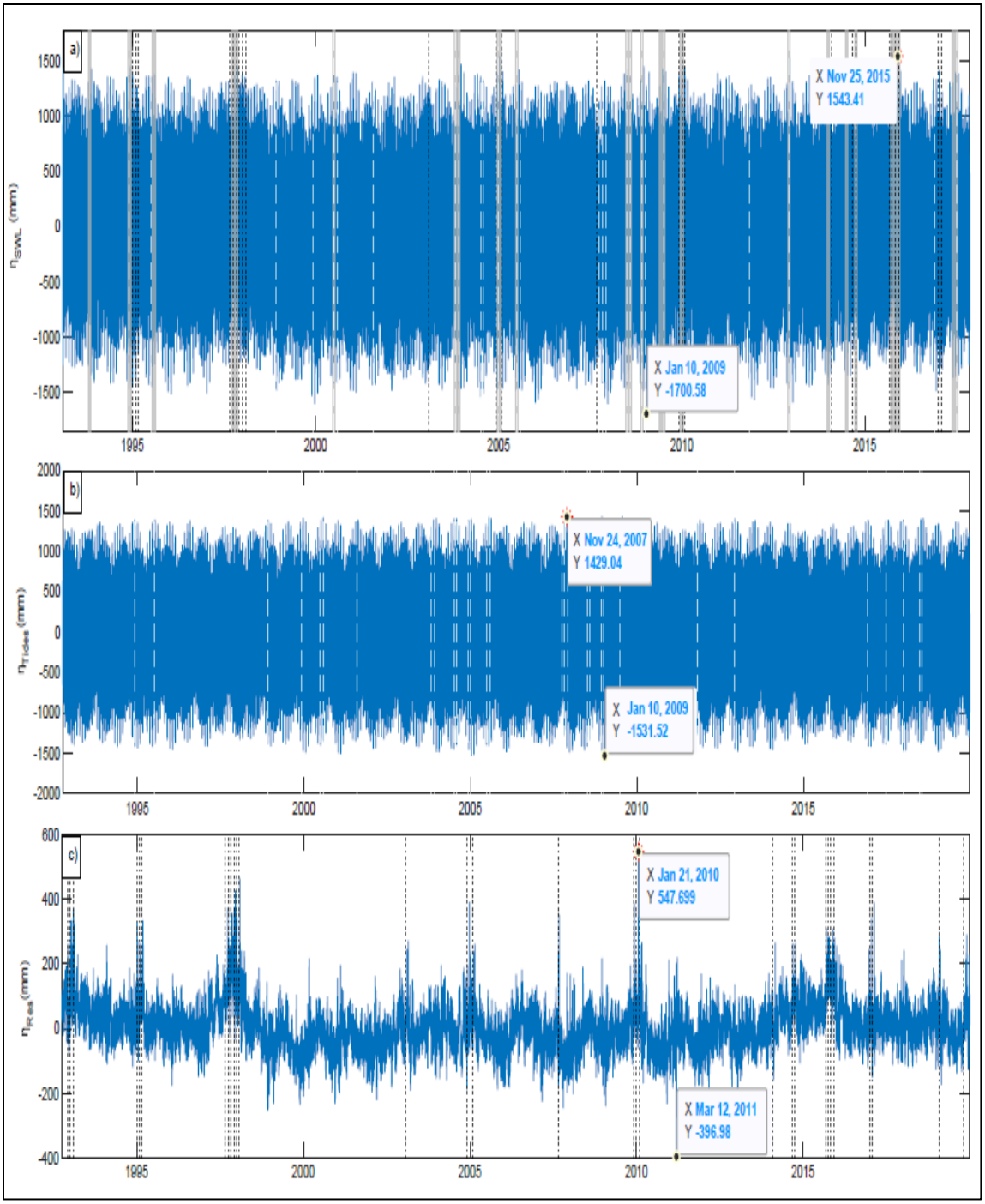

Station 9410170 SWL timeseries. a) SWL, b) tidal fit, and.c) residual timeseries with minimum and maximum (red asterisk) levels noted. 30 largest events highlighted for SWL (gray lines), tides (white dash lines) and residual (dotted black lines).

Figure 4. San Diego Coastal Sea Level Timeseries

Hourly detrended still, tidal, and non-tidal water levels were also calculated for La Jolla, where SWL timeseries has a 3119 millimeters (mm) range (-1613 mm on 04 January 2006 to 1506 mm on 25 November 2015), 225 mm smaller than San Diego; the tidal components range is 2786 mm (-1427 mm on 11 January 2005 to 1359 mm on 22 July 2009), 273 mm smaller than San Diego; Non-tidal components of SWL range from 820 mm (-250 mm on 04 January 2006 to 570 mm on 22 December 1997), 227 mm smaller than San Diego. The five-day detrended SSHA from altimeter data for a grid point centered at 33° 45.0′ North, 117° 45.0′ West, revealed a much smaller 226 mm water level range (-80 mm on 07 February 2002 to 146 mm on 17 October 2015), an expected result owing the altimetry poor temporal resolution. Interestingly, the highest SWL was recorded at the same time for both stations indicating similar processes influence water levels at both locations; San Diego lowest SWL and tidal levels occurred at the same time, indicating the large tidal influence on SLV; and La Jolla lowest SWL and non-tidal levels occurred at the same time, indicating that non-tidal phenomena ha a large influence at that location.

Comparison of the 30 largest levels for each component at both locations, showed that for San Diego 14 maximum tidal events are aligned with SWL maximum events, and nine maximum non-tidal events aligned with maximum SLW. The dates of these events are denoted in Table 2, which is organized by years along the rows and months in the columns. A red “R” indicates the month/year pair during which one of the 30 maximum residual water levels was observed. Blue text denotes that calendar day of the month/year pair that the tidal component was maximum. For example, a tidal maximum occurred on 12 July 1995. Gray boxes indicate month/year pairs when total SWL reached a maximum. At La Jolla, 18 maximum tidal events that are aligned with SWL maximum events, and eight maximum non-tidal events align to maximum SLW. For the SOCAL area, the 10 largest levels are accumulated over 1997–1998 and 2015. The largest tidal events show 28-day, semiannual, and interannual periodicity, and the largest non-tidal events are mainly accumulated over 1993, 1997, 2010, and 2015. The water level time series indicate that tides are the main contributor to water levels in the study area with a suspected peak of the 18.6-year cycle between 2008 and 2009. The spectra do not validate the 18.6-year cycle as U-tides may not be able to calculate this accurately. Periodicity of tidal components points

to spring tides as the main exacerbating phenomena; however, there is a significant contribution from non-tidal events that added to tides, which led to the maximum water levels. In other words, the highest observed water levels occurred when non-tidal events occurring during periods when the tidal component of the water level was also high. It is suspected that forcing of 2015 largest SWL event is a combination of spring tides and residual influences. The agreement of magnitudes and occurrences indicate validity of the comparison from a regional perspective and provides defined level of detail inherent to each location.

Sea level trend was calculated for two time periods. A 40-year period from 01 January 1980 to 31 December 2019 revealed a 2.48 mm $year^{-1}$ (1.9 mm $year^{-1}$) trend for San Diego (La Jolla). The 26-year period trend from 02 October 1992 to 31 December 2019 was 2.83 mm $year^{-1}$ (2.63 mm $year^{-1}$) for San Diego (La Jolla). The NOAA CO-OPS (NOAA Tides and Currents 2022) San Diego relative sea level trend is 2.2 mm $year^{-1}$ based on monthly sea level data from 1906 to 2021 and is 2.04 mm $year^{-1}$ at La Jolla based on monthly data from 1924 to 2021. SOCAL sea level trend is 1.64 mm $year^{-1}$ based on SSHA data from October 1992 to January 2019. There is a consistent slope increase over time on tends in San Diego, the location most exposed to anthropogenic influences (such as the man-made harbor and silver strand); a small decrease, followed by a steep increase over the three periods in La Jolla; and comparing the trends for all locations, SOCAL has the lowest rise rate, which is an indication that tidal or transient processes drive SLR in the region. These trends highlight an accelerating rise rate, especially in the altimeter era, which has been discussed in other studies.

Table 2. Maximum Recorded Levels

	Jan	Feb	Mar	Apr	May	Jun	Jul	Aug	Sep	Oct	Nov	Dec
1992												R
1993	R	R										
1994												03T
1995	R	R	R				12T					
1996												
1997									R	R	R	R
1998	R	R										04T
1999												23T
2000							03T 31T					
2001								19T				
2002												
2003		R									24T	23T
2004							03T 31T					06R 12T
2005	10T	R					22T	19T				
2006												
2007								R	R	27T	24T	23T
2008							03T	01T				12T
2009	10T						22T			R	R	R
2010	R											
2011											25T	
2012												13T
2013												
2014										R		
2015									R	R	R	R
2016												13T
2017	R	R					23T					
2018	02T						14T	11T				
2019		R									R	

R: Residual maximum event, ##T: Tidal maximum event with date. Gray shaded cell: SWL maximum event.

After assessment of large tidal and non-tidal components, the seasonal analysis facilitates interpretation and effect of filtered processes. Figure 5 shows the seasonality composition for San Diego and La Jolla. San Diego SWL (Figure 5a) seasonality range is 174 mm (-91 mm in April to 83 mm in September), composed by a tidal seasonality (Figure

5b) range of 155 mm (-79 mm in April to 76 mm in September) added to the non-tidal seasons (Figure 5c) range of 29 mm (-15 mm to 14 mm with three oscillations cresting in January, May, and September). La Jolla SWL (Figure 5d) seasonality range is 179 mm (-94 mm in April to 85 mm in September), composed by a tidal seasonality (Figure 5e) range of 156 mm (- 79 mm in April to 77 mm in September) added to the non-tidal seasons (Figure 5f) range of 30 mm (-16 mm to 14 mm with three oscillations cresting in January, May, and September). There is good agreement on magnitude and time for San Diego and La Jolla water levels seasonality, with most of the contribution matching SA (primarily) and SSA tidal fits as confirmed by the spectra (Appendix).

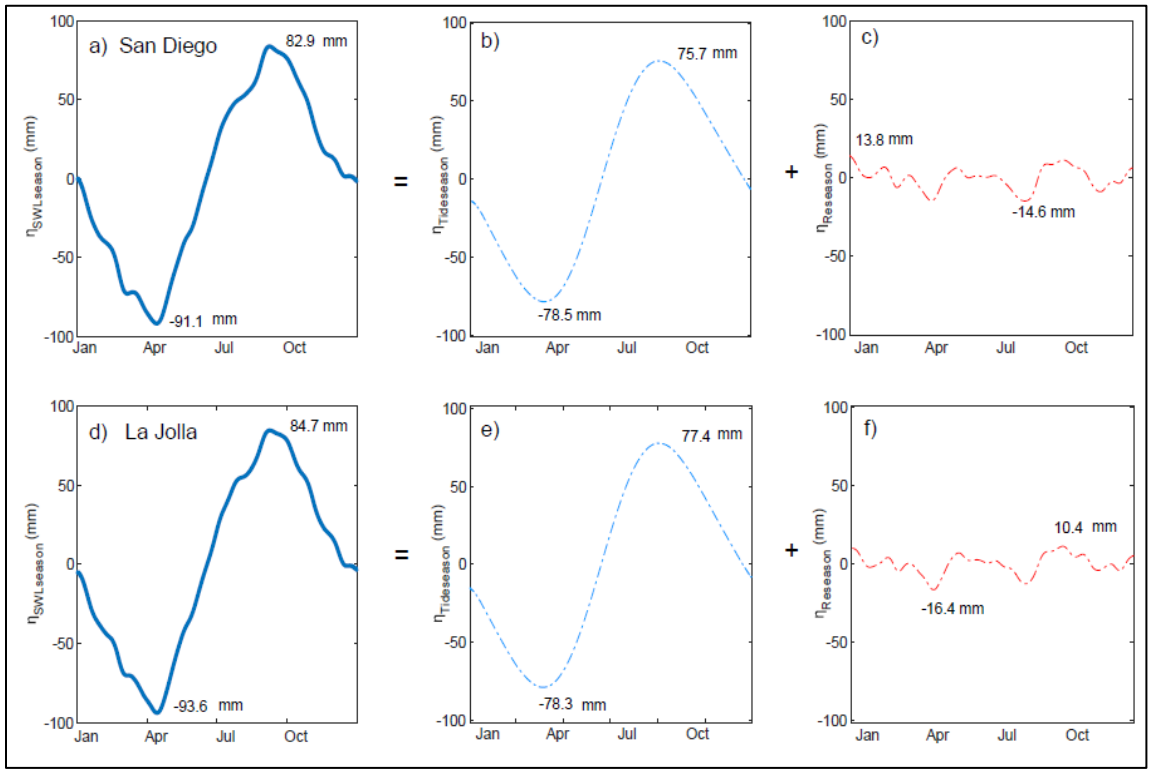

Average seasonal components of a) San Diego SWL (blue solid line), b) San Diego tidal fit (blue dashed line), c) San Diego residual (red dash line), d) La Jolla SWL (blue solid line), e) La Jolla tidal fit (blue dashed line), and f) La Jolla residual (red dash line). Units are represented in mm. Lowest and largest values noted. The leftmost panel in each row in equivalent to the sum of the two panels to the right of the equality sign.

Figure 5. SWL Seasonality Composition

Comparison of seasons for all locations is shown in Figure 6. There is good agreement on magnitude and time on seasons for San Diego and La Jolla. The altimetry seasonality with a range of 69.5 mm, was 61% lower in magnitude with a 2- to 4-week lag from SWL seasons, which indicates different open ocean processes could be influencing seasonality at the regional level or that altimetry cannot observe amplification at the coast. The non-tidal components presented in Figures 5c and 5d, have seasonal maxima and minima that temporally aligned with altimetry seasonality (April and October).

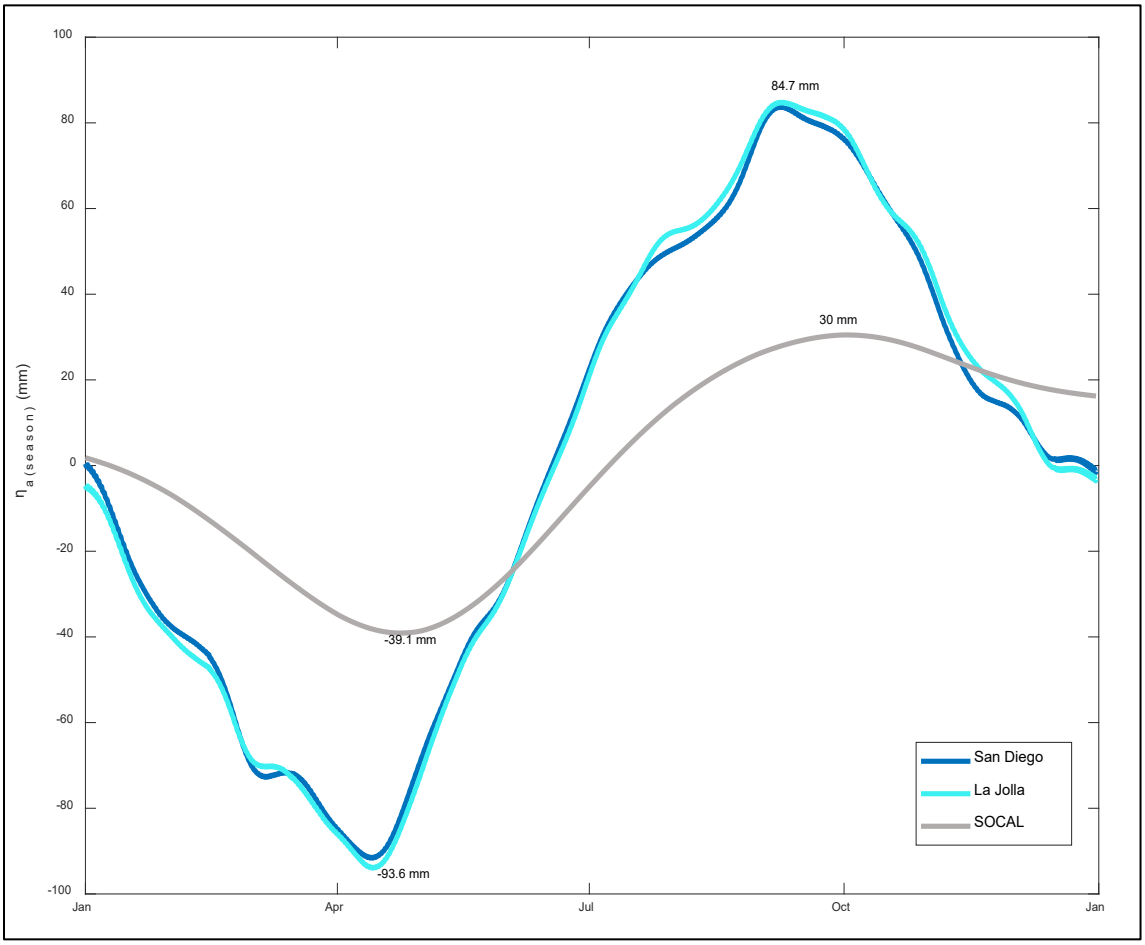

Average seasonal magnitudes for a) San Diego SWL, b) La Jolla SWL, and c) SOCAL SSHA, are represented in mm. Lowest and largest values noted.

Figure 6. Sea Level Seasonality

C. NON-TIDAL COMPONENTS

Further evaluation of the residual SLW component and SSHA led to measurement of five non-tidal events with good agreement for the three locations (Figure 7). Figure 7a and Figure 7b show the detrended, residual component of San Diego and La Jolla SWL respectively with seasons removed, including the 30 largest water level events (grey lines) to visually contrast individual contributions. Compared to Figure 4c (SWL with seasons), there is minimal change in Figure 7a due to the small magnitude of the non-tidal seasons. Figure 7c shows the detrended, de-seasoned SOCAL SSHA.

Figure 7d shows that at San Diego, transient events contributed to the total water level across a range of 713 mm (-328 mm to 385 mm) with the maximum value recorded on 04 September 2007. For La Jolla (Figure 7e), transient events contributed to a water level range of -490 mm to 351 mm (841 mm range) with the maximum value recorded on 01 July 2007. It is noted a larger magnitude for transient events in La Jolla, highlighting the differences of processes at an open beach opposed to an enclosed basin, perhaps due to direct exposure to set up and swash. The enlarged pattern transient phenomena every winter, aligns with the times of increased precipitation in California (potentially exacerbated by atmospheric river events). The SOCAL transient-filtered time series contained negligible components because the temporal resolution of the altimeter data was only 5 days; this component was not further analyzed (Figure 7f); however, it is expected for the magnitudes of the altimeter and gauge data to become closer as they are filtered for lower frequency variability.

Figure 7g, Figure 7h, and Figure 7i, show the S2S components of water levels for San Diego, La Jolla, and SOCAL respectively, with good agreement in magnitude for the tide gauges. San Diego S2S range was 242 mm (-128 mm to 114 mm) with the maximum value recorded on 02 March 2001; La Jolla had a range of 271 mm (-161 mm to 110 mm) with the maximum value recorded on 05 January 1998; and SOCAL had a range of 103 mm (-41 mm to 62 mm) with the maximum value recorded on 13 July 2017. The occurrence of maximum S2S level is different for each time series, an indication that intrinsic coastal processes local to a specific area impact water levels at fine spatial scales after they are more uniformly affected over a larger region by sub-seasonal processes.

Figure 7j shows San Diego S2A events with a range of 114 mm (-49 mm to 65 mm) with the maximum value recorded on 16 August 1998. For La Jolla (Figure 7k), S2A events had a 123 mm range (-51 mm to 72 mm) with the maximum value recorded on 23 November 1997. For SOCAL (Figure 7l), S2A events had a 70 mm range (-35 mm to 35 mm) with the maximum value recorded on 10 December 1997. Maximum S2A levels occurrence aligns for SOCAL and La Jolla, and are only one year apart from San Diego, potentially due to larger scale alignment of lower frequencies; in other words, longer term events tend to match spatially as if they were averaged over altimeter scales rather than point measurements.

Figure 7m, Figure 7n, and Figure 7o, show the IA component of water levels, for San Diego, La Jolla, and SOCAL respectively. San Diego IA range is 213 mm (-69 mm to 144 mm) with the maximum value recorded on 15 November 1997; La Jolla has a range of 219 mm (- 75 mm to 144 mm with the maximum value recorded on 29 October 1997; and SOCAL has a range of 144 mm (-47 mm to 97 mm) with the maximum value recorded on 07 October 2015. Maximum S2A levels magnitudes and occurrence aligns for San Diego, La Jolla and the second largest value for SOCAL.

Figure 7p shows San Diego decadal events with a range of 32 mm (-10 mm to 22 mm with the maximum value recorded on 27 February 2019. For La Jolla (Figure 7q), S2A events have a 20 mm range (-9 mm to 11 mm with the maximum value recorded on 21 July 2016. For SOCAL (Figure 7r), decadal events have a 31 mm range (-12 mm to 19 mm) with the maximum value recorded on 10 March 2018. Although, maximum decadal levels agree on magnitude and occurrence for all sites, caution must be used when analyzing decadal timeseries due to the limited sample size as bias can be induced with only 26 years of data. Probability distribution of non-tidal components was calculated, and the decadal component did not have a normal distribution (See Appendix).

It is interesting how S2S, S2A and IA maximum events at La Jolla, occurred at the same time and align with some of the largest residual and SWL events, indicating that non-tidal forces can become a SLV driver in the study area. Spectral analysis validated that the primary source of SLV originates from tidal components, followed by IA and transient components; filters comparison indicates, the largest variability influence is from a

combination of transient and inter-annual events at shore locations, and IA events for the SOCAL area (Appendix).

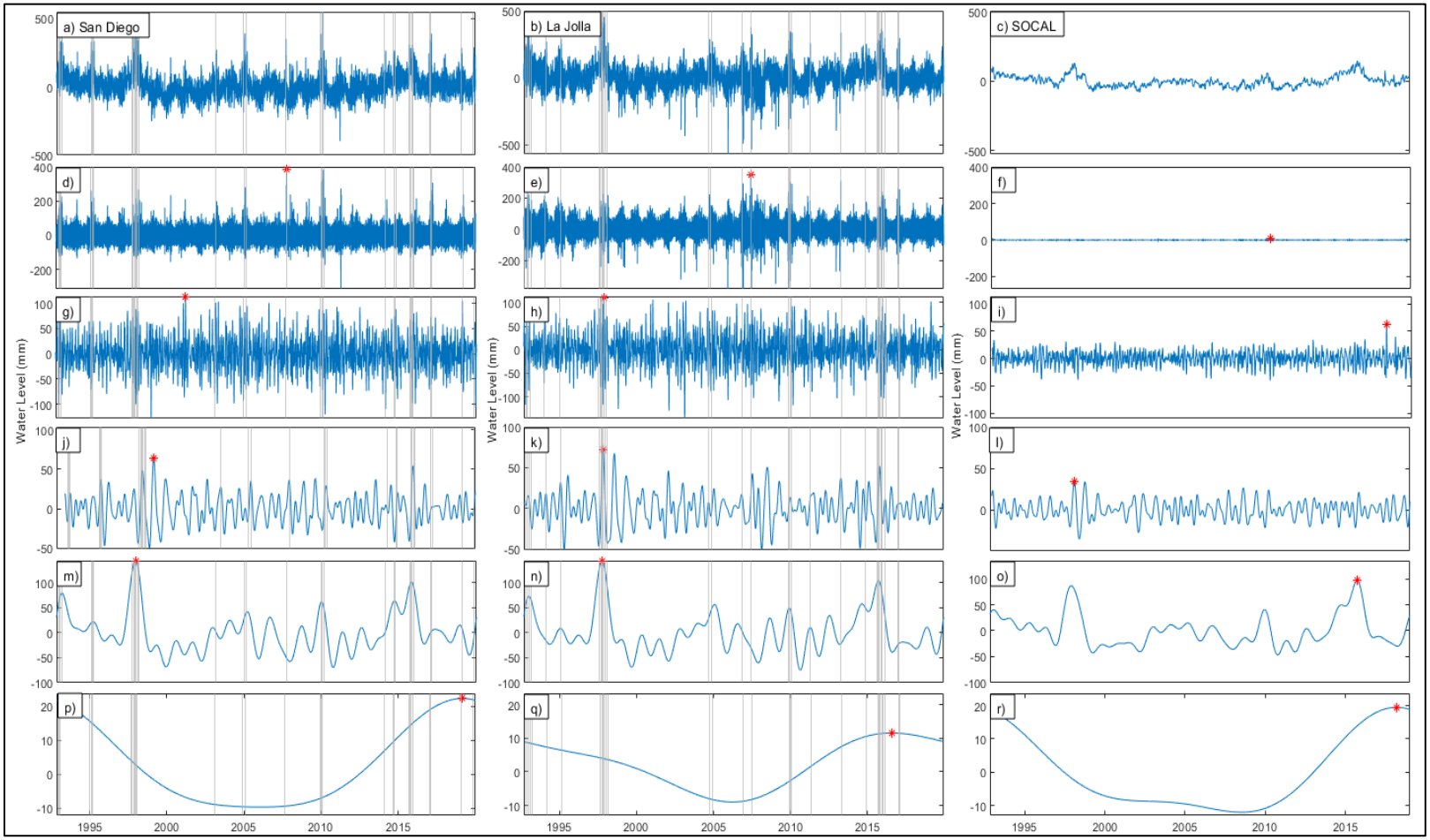

Filtered non-tidal components of detrended, de-seasoned a) San Diego η_{Res}, b) La Jolla η_{Res}, and c) SOCAL $\eta_{a,}$ timeseries represented by transient (d, e, and f), S2S (g, h, and i), S2A (j, k, and l), IA (m, n, and o), and decadal (p, q, and r) events, respectively. Maximum Seal Level recorded (red asterisk). SWL residual 30 largest events depicted (gray lines).

Figure 7. Non-tidal Component Filters

D. SLV CONTRIBUTORS

Further analysis of the contributions of each non-tidal component led to the development of a SLV "thumbprint" with the interaction and contribution of each component. Figure 8 shows the SWL contributors stacked plots for San Diego (Figure 8a) and La Jolla (Figure 8b). San Diego featured a 1127 mm SWL 99th percentile, a 1016 mm tidal 98th percentile, and a 198 mm residual 99th percentile. There were 40 instances when the water level from combined components was above 1431.8 mm, exceeding the SWL 99Th percentile by at least 304 mm (one foot). Figure 8b shows the La Jolla SWL "thumbprint." It depicts a 1068 mm SWL 99th percentile, a 957 mm tidal 98th percentile, and a 197 mm residual 99th percentile. There were 48 instances when the water level from combined components was above 1372.8 mm, exceeding the SWL 99Th percentile by at least one foot.

Figure 9 shows a stacked plot of the sea level compiled contributors after tides were removed. Figures 9a and 9b show San Diego and La Jolla unique "thumbprints," respectively, with a -138 mm (-156mm) residual 1st percentile at San Diego (La Jolla). When the tidal component was removed from the SWL, there were 231 (279) times in San Diego (La Jolla) where the combination of non-tidal components contributed to an increase of water levels, 26 (33) of those above the 99th residual percentile; and 53 (23) events where residual components generated a decrease of water levels in San Diego (La Jolla). There is a noticeable IA influence throughout the time series that contrasted to the red lines in Figure 8, corroborates that those extreme events are not only tidal in nature but are intensified by non-tidal components. Looking at the occurrence of extreme events by time, there were 72 (56) positive and 7(3) negative contributions at San Diego (La Jolla) from years 1992 to 2000; 61 (130) positive contributions and 35 (12) negative contributions at San Diego (La Jolla) from years 2000 to 2010; and 98 (71) positive contributions with 11 (7) negative contributions at San Diego (La Jolla) from 2010 to 2019. In the past three decades La Jolla experienced more intense extreme events in the 2000–2010 period, whereas at San Diego, the number of extremes has increased during the last decade (2010–2020) likely owing to enhanced wave-driven water levels on the open coast (La Jolla).

Figure 9c shows SOCAL unique “thumbprint” with a 118 mm sea level 99th percentile, and a -69 mm sea level 1st percentile. Stacked individual contributors corroborates the large Inter-annual influence observed at La Jolla and San Diego, confirmed by spectral analysis with IA $\kappa\sim$ 0.775, followed by 0.627 for season, 0.51 for decadal events, 0.303 for S2A and 0.274 for S2S. The large contribution of tides diffuses the SWL response to induvial contribution in the spectral analysis. (Appendix)

The unique sea level composition reveals subtle characteristics of SLV at each location; while there are evident inter-annual and seasonal effects in addition to the large tidal influence, the magnitudes, and patterns of transient, S2S, S2A, and decadal components seems to drive variability in an exclusive way.

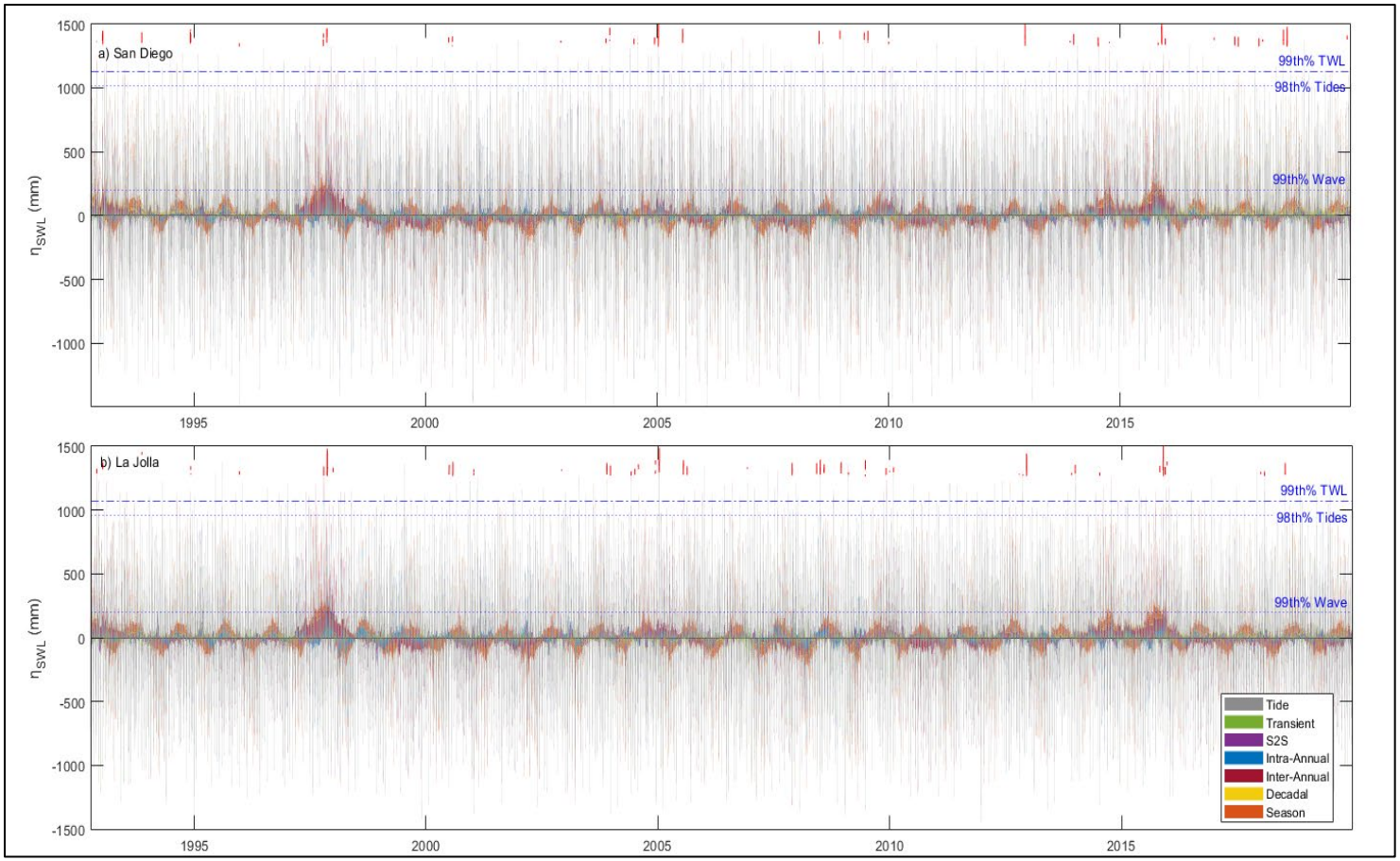

SWL "thumbprints" unique to a) San Diego, and b) La Jolla, represented in a fishbone of compiled contributors from 1992 to 2019. SWL 99th % (blue dash lines), tides 98th percentile and residual 99th percentile (blue dash lines) noted. Water Level exceeding one foot above SWL 99th percentile (red).

Figure 8. SWL Stacked Contributors

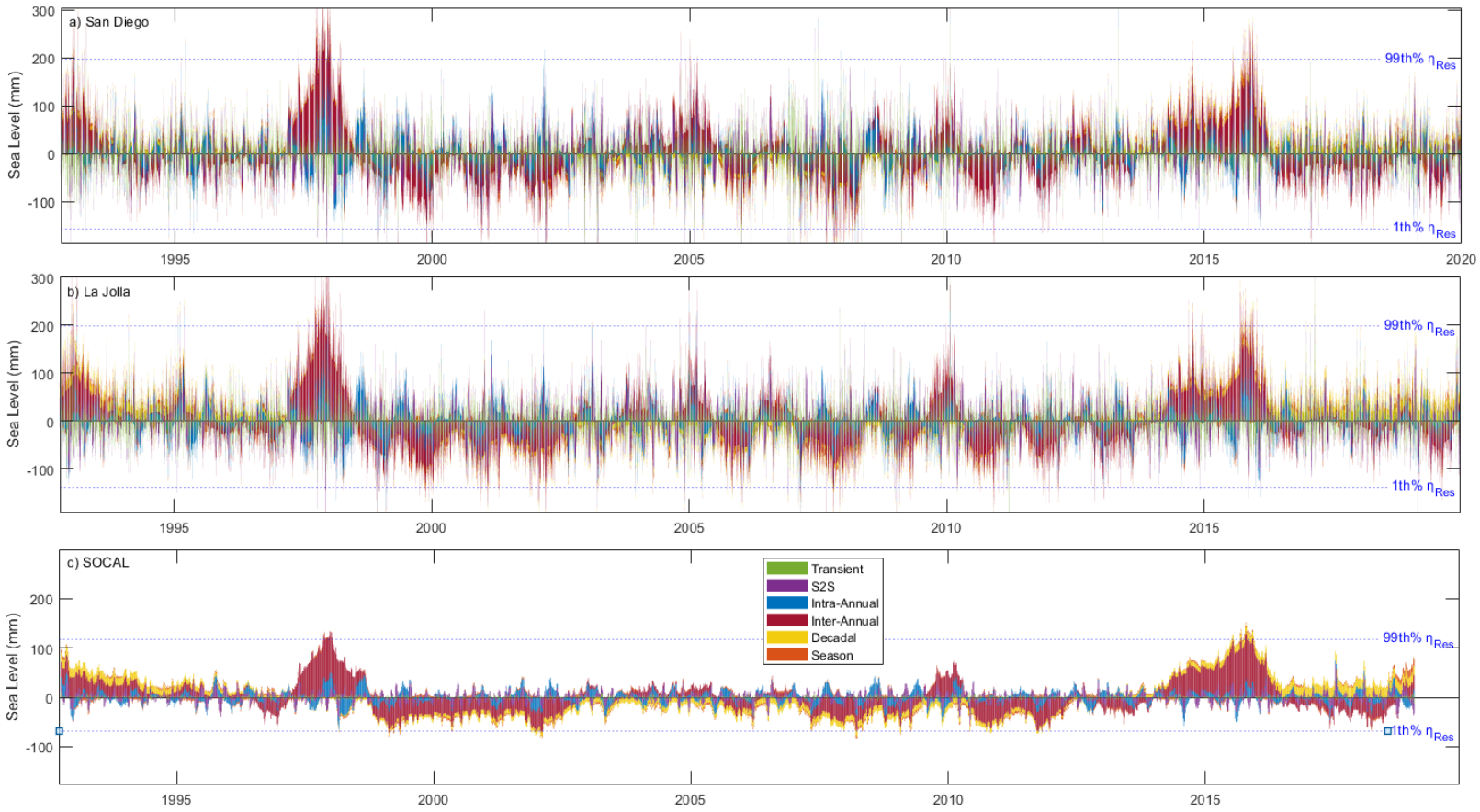

Sea level "thumbprints" unique to a) San Diego, b) La Jolla, and c) SOCAL represented in a fishbone of compiled contributors from 1992 to 2019. Non-tidal components 1 and 99th percentile (blue dash lines) noted.

Figure 9. Sea Level Stacked Contributors

Detailed analysis of San Diego non-tidal and seasonal contributions with SLV that exceeded the 99th percentile of water levels is derived from Figure 9a and presented in Figure 10. Figure 10a highlights the areas where large variability was registered for the entire timeseries displayed in Figure 9a. These periods were

1. October 1992–February 1994 (Figure 10b), which contained a positive IA and decadal contribution;
2. February 1997–July 1998 (Figure 10c), which contained a significant IA contribution supported by S2A events at the peak;
3. September 2004–May 2006 (Figure 10d), which highlighted a pattern shift driven by IA events;
4. March 2009–March 2011 (Figure 10e), which was the largest observed residual event supported by positive contributions from transient, S2S, S2A, IA, and seasonal variability; and
5. February 2014–May 2016 (Figure 10f), which featured a large IA contribution.

Figure 11 is similar to Figure 10 but instead highlights periods of low SLV that in some cases reached below the 1st percentile of water levels. Figure 11.b shows individual SLV contributions from August 1998 to February 2003 with negative IA contributions throughout the entire period and a decadal shift from positive to negative. Figure 11.c shows individual SLV contributions from September 2007 to August 2008 with large IA influence and transient contribution to below 1st percentile events. Figure 11.d illustrates individual SLV contributions from January 2017 to December 2019, highlighting minimal IA contribution and positive decadal contribution.

A particular finding is that S2S phenomena consistently was the prevailing variability driver by either constructive or destructive interference as it propelled water level patterns. The spectra (presented in the Appendix) corroborated that IA levels had the largest contribution; decadal variability was small in magnitude but had an interesting effect and relationship to IA; seasonality, S2A and transient events aid in exhilaration of

water levels; inspection of the La Jolla and SOCAL “thumbprints” yield to the same result. Speculatively, the strong S2S contribution may be related to coastally trapped Kelvin waves propagating through the California Current System (Amaya et al. 2021) after equatorially trapped Kelvin waves generated in the MJO are deflected poleward after colliding with the South American land mass.

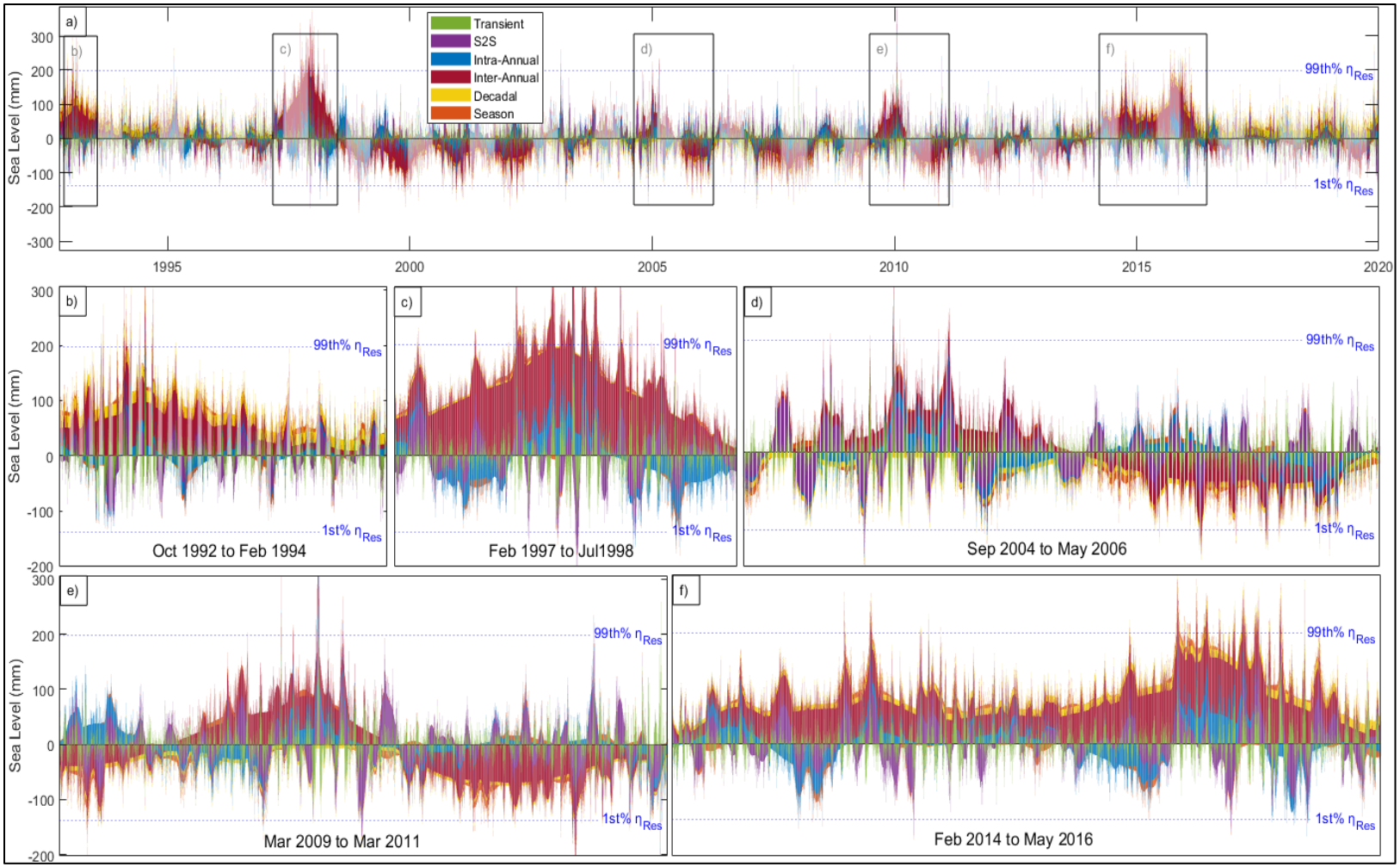

Sea level "thumbprint" unique to San Diego with a) overall areas of large variability indicating specific time frames from b) 1992 to 1994, c) 1997 to 1998, d)2004 to 2006, e) 2009 to 2011, and f) 2014 to 2016, represented in a fishbone of compiled contributors. Non-tidal components 1st and 99th percentile (blue dash lines) noted.

Figure 10. San Diego Large SLV

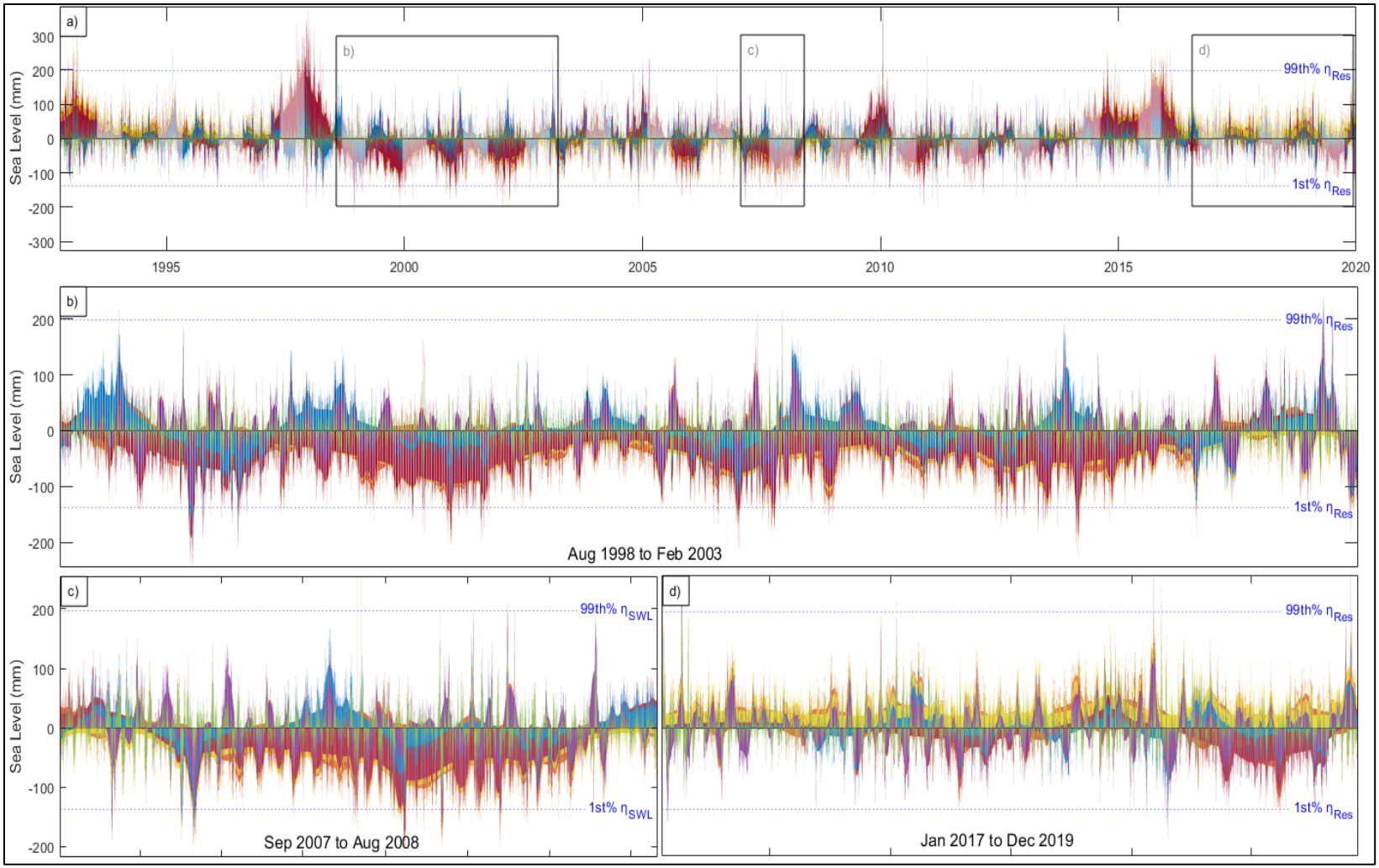

Sea level "thumbprints" unique to San Diego with a) overall areas of low variability indicating specific time frames from b) August 1998 to February 2003, c) 2007 to 2008, and d)2017 to 2019, represented in a fishbone of compiled contributors. Non-tidal components 1st and 99th percentile (blue dash lines) noted.

Figure 11. San Diego Low SLV

E. MAXIMUM WATER LEVELS

To represent the annual cycle of SLV extremes, we can view the maximum magnitude of the tidal and each non-tidal component when super-imposed onto each other to denote a maximum possible water level if all components were simultaneously and positively impacting total water level. Figure 12 shows such a SWL extreme scenario as a function of month using the maximum water levels recorded from 1992–2019. San Diego EWL ranged from 1638 mm at its lowest in May to 2067 mm in January and 2043 mm in September at its highest (Figure 12a). Tides (light blue) had a 244 mm variability, ranging from 1188 mm in March to 1442 mm in July. In other words, the highest tide observed in July was 244 mm higher than the highest tide observed in March. Transient events (green) had the largest variability (258 mm) ranging from 127 mm in May to 359 mm in September and up to 385 mm in January, which is expected owing to seasonal variability of wave events. S2S variability (purple) was between 70 and 105 mm, intra-annual (dark blue) ranged between 28 and 63 mm; inter-annual (red) between 54 to 140 mm, and the decadal (yellow) maximum contribution was 22 mm throughout the year. Figure 12.b shows the same figure from La Jolla: EWL there ranged from 1528 mm at its lowest in March to 1911 mm in January and 1969 mm in July at its highest; tides had a 256 mm variability ranging from 1096 mm in March to 1352 mm in July. Transient events had the largest non-tidal variability (219 mm) ranging from 200 mm in April to 305 mm in January and up to 319 mm in July. S2S variability was between 70 and 111 mm, S2A variability was between 25 and 71 mm, IA variability ranged between 54 and 141 mm, and the decadal maximum contribution was 11 mm throughout the year.

Figure 13 is the same as Figure 12 but shows sea levels extreme scenarios as a function of month with tides removed, using the maximum water levels recorded from 1992–2019. Figure 13a depicts San Diego non-tidal and seasonal combined contributions ranging from 329 mm in May to 720 mm in October. Figure 13b depicts La Jolla non- tidal and seasonal combined contribution ranging from 402 mm in April to 617 mm in July. SOCAL EWL ranged from 149 mm at its lowest in April to 213 mm in October at its highest (Figure 13c). IA events (red) had the largest variability ranging from 67 mm in April to 98 mm in October, S2S variability (purple) was between 24 and 44 mm being

lowest in January and largest in July; S2A variability (dark blue) was between 22 and 34 mm being lowest in April and largest in December, and the decadal (yellow) maximum contribution was 20–21 mm throughout the year; transient-contributions (green) are negligible as a result of low temporal resolution of the altimeter data.

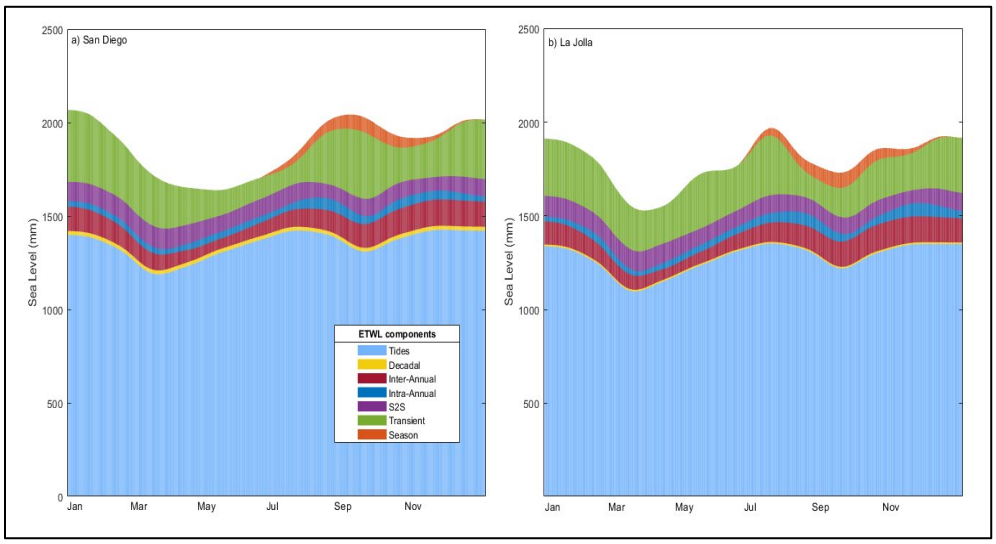

Maximum SWL for a) San Diego, and b) La Jolla, in a year are represented by color-coded combination of factors using levels recorded from 1992 to 2019.

Figure 12. SWL EWL Components

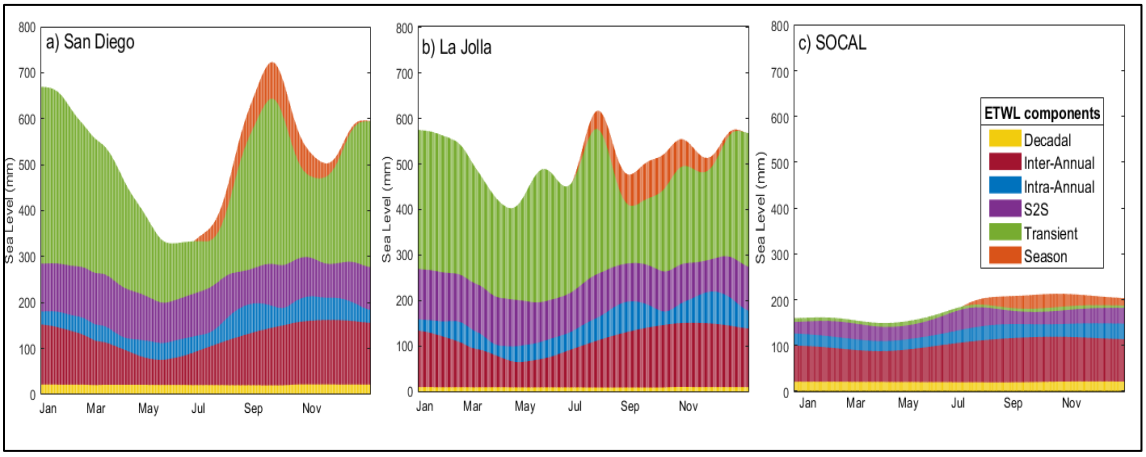

Maximum sea level (tides removed) for a) San Diego, b) La Jolla, and c) SOCAL in a year are represented by color-coded combination of factors using levels recorded from 1992 to 2019.

Figure 13. Sea Level EWL Components

San Diego and La Jolla EWL indicate that the maximum water level in a year is close to 2000mm (over for San Diego, under for La Jolla), results that agree with the levels presented in sections 4.b and 4.d. The combination of tidal maxima, transient maxima and IA maxima produced the most significant variability which could be presented as stronger than normal surge or wave setup, a product of processes enhanced by an inter annual phenomena. The contrast between coastal and open ocean non-tidal contributions presented in Figure 12 reveals the influence of transient events that are more significant at San Diego but have more variability at La Jolla. Figure 13 reveals the influence of inter-annual events that tend to be larger in magnitude at San Diego. All locations show good agreement on IA, S2S, S2A, seasonal and decadal, order of magnitude magnitudes and patterns.

F. CLIMATE-DRIVEN SLV

To determine the potential of climate related drivers in the San Diego area, an initial monthly correlation analysis indicated significance for climate modes relation to SLV, especially for the PDO and the indices presented in Table 1. Further analysis was performed using the non-tidal and seasonal daily water level components from 1981–2019.

Figure 14 shows the Pearson correlation coefficient (ρ) between individual water levels and daily climate indices. The 95% significance level ($\rho_{95\%}$) was about 0.027, and any correlation not meeting this significance falls within the red dashed lines. Figure 14a shows ρ for San Diego individual SLV components related to AO, AAO, NAO, PNA, and Niño 3 indices. Figure 14b shows ρ for San Diego individual SLV components related to the 10 MJO time-lagged patterns.

San Diego station shows the largest statistically significant correlation of Inter-Annual SWL to the Niño 3, Niño 3.4, and Niño 4 ($\rho \sim 0.53$ to 0.756); an intermediate positive correlation with MJO 2, MJO 3, MJO 4, and MJO 5 ($\rho \sim 0.22$ to 0.3); an intermediate negative correlation with MJO 7, MJO 8, MJO 9,and MJO 10 ($\rho \sim -0.3$ to -0.16); and a weaker but statistically significant correlation with the AO, AAO, PNA, MJO 1 and MJO 6 ($\rho \sim -0.07$ to 0.12). A notable feature is that the largest correlation for San Diego is with the ENSO and indicates that majority of inter annual influence is due to this

climate mode, corroborating that the events highlighted in Figure 3 and Figure 10 are ENSO events for the years 1997 and 2015. It is also evident the largest response of decadal SWL is to Niño indices, which is consistent with the understanding of a relationship between PDO and ENSO. It is also suspected that some S2A events are capturing the lowest periodicity of ENSO. With respect to the MJO, an interesting finding is that even though it is classified as an intra-seasonal oscillation, the largest response is from IA events with significance for all MJO patterns, followed in magnitude and pattern by S2S and decadal events. The cyclic pattern response of S2A and seasonal water levels to the MJO indices is opposite to the IA, S2A and decadal.

Figure 15 shows ρ and κ between water levels and daily climate indices. The 95% significance levels are $\kappa_{95\%} \sim 0.38$ and $\rho_{95\%} \sim 0.027$. Any correlation not meeting this significance falls within the red dashed lines. Figure 15a shows the ρ value for San Diego SWL related to climate indices. Figure 15b shows the κ value for SOCAL related to climate indices. San Diego station shows the largest statistically significant response of SWL to the Niño 3, Niño 3.4, and Niño 4 ($\rho \sim 0.36$ to 0.41); intermediate positive correlations with MJO 2, MJO 3, MJO 4, and MJO 5 ($\rho \sim 0.12$ to 0.18); intermediate negative correlations with the MJO 7, MJO 8, MJO 9, and MJO 10 ($\rho \sim -0.18$ to -0.08); and weaker but statistically significant correlations with the AO, NAO and MJO 1 ($\rho \sim -0.07$ to 0.05). Interestingly, the San Diego SWL (117°W) response to the MJO 6 (120°W) is not significant, and response to the MJO patterns 7–10 is negative, indicating that enhanced precipitation is equivalent to low SLV or vice versa. The negative SWL response to the AO is suspected to be driven by coupled S2S, S2A and SA processes as the annular pattern has large variability, and the negative response to NAO is suspected to be driven by seasonal patterns as a teleconnection to atmospheric phenomena in the north Atlantic basin.

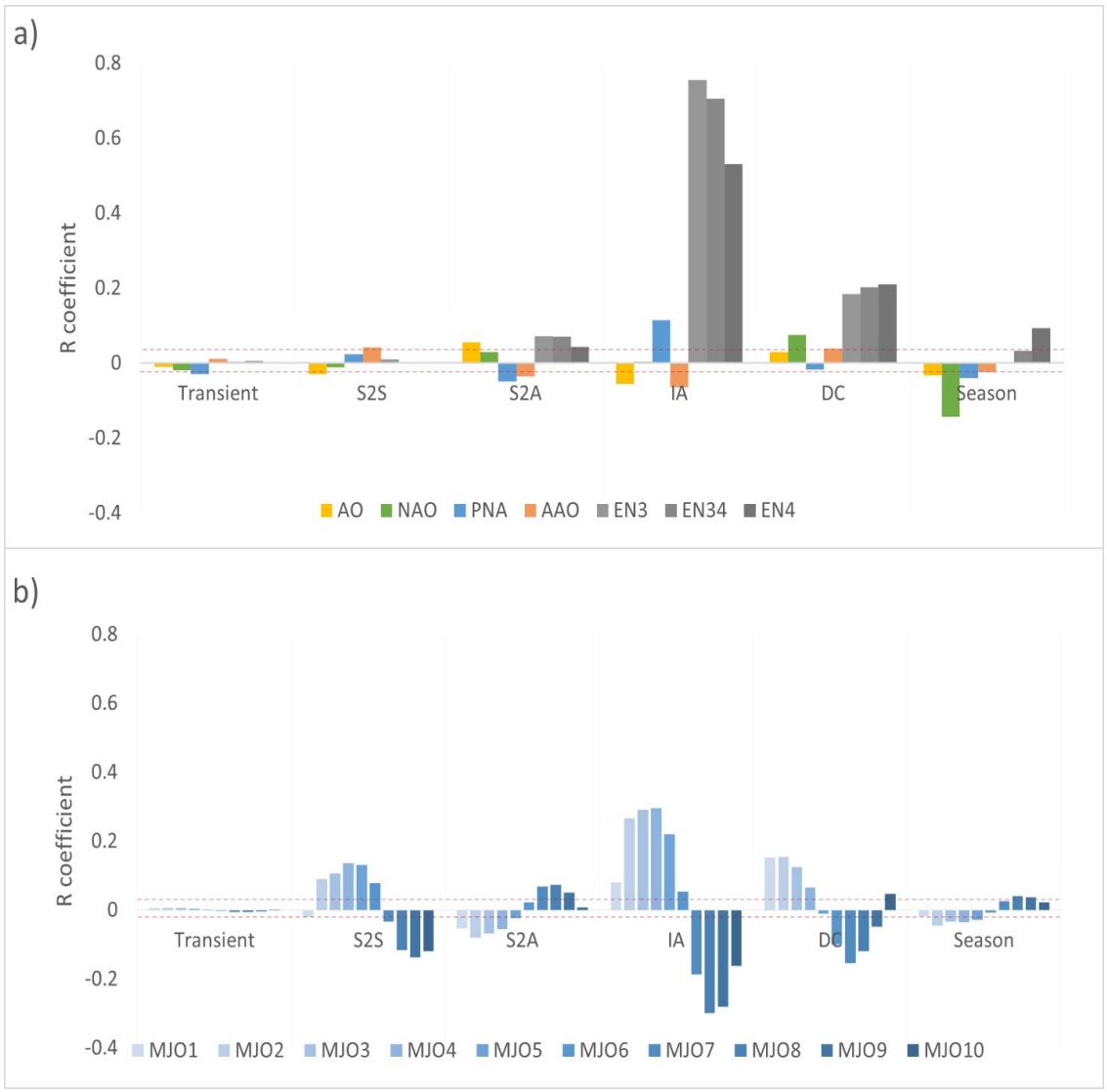

Correlation coefficients between individual water levels and daily climate indices (colored bars). a) The strength of the linear relationship between SWL individual components and the AAO, the AO, the NAO, the PNA, the ENSO, and b) the MJO is represented by ρ. The 95% significance level is $\rho_{95\%}$~0.027(red dashed lines).

Figure 14. San Diego SLV Components Relationship to Climate Modes

The SOCAL area shows statistically significant coherences between SSHA and the Niño 3, Niño 3.4, Niño 4, MJO 2, MJO 3, MJO 4, MJO 7, MJO 8, and MJO 9 indices ($\kappa \sim$ 0.43 to 0.56). coherence between Niño indices and SSHA are consistent with the IA variability observed in SWL, an expected result for East Pacific coastal regions as mentioned in Chapter II. The coherence between SSHA and the MJO indices is consistent

with the SWL cyclic pattern in correlation, but κ magnitudes are as large as the coherence with ENSO indices, potentially due to the difference between coastal processes and open ocean forcing or to the inconsistent spatial resolutions between altimetry and tide gauges.

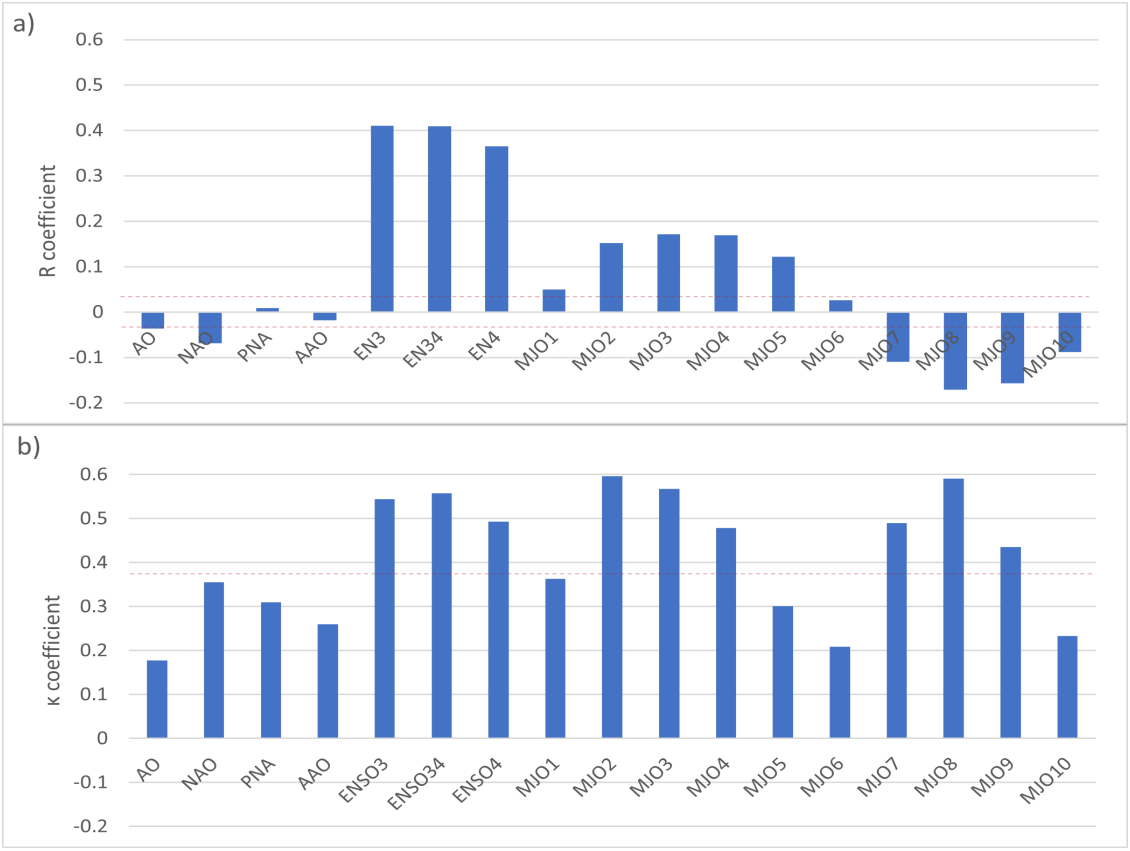

ρ and κ between water levels and daily climate indices. a) The strength of the linear relationship between San Diego SWL individual components and the AAO, the AO, the NAO, the PNA, the NIÑO, and MJO is b) The proportion of the standard deviation of SOCAL sea level accounted for by the AAO, the AO, the NAO, the PNA, the ENSO, and MJO is represented by κ. The 95% significance levels are $\kappa_{95\%} \sim 0.38$ and $\rho_{95\%}$~0027 (red dashed lines).

Figure 15. California SLV Relationship to Climate Modes

G. PROOF OF CONCEPT SUMMARY

Overall, the proof-of-concept analysis revealed that tides (primarily spring tides) are the SLV driver at coastal southern California, followed by IA processes (mainly ENSO). Transient components are of influence at coastal levels but some of the processes

that follow under that periodicity are different for enclosed harbors than for open beaches. Even when tidal and coastal processes complexities are removed, inter-annual events exacerbate water level variability pointing to ENSO is the core climate SLV driver for the area is, followed by some MJO influence (which is stronger at coastal areas), matching the consistent flooding and strong tides phenomena observed in San Diego County. The implications of these results mean that the unique "thumbprints" facilitate decision-making processes by informing planners on when, how, where and what contributes to SLV. If all components' maxima were to align, a total of 2247 mm could be reached, and that approximation in conjunction with regional SLR scenarios should become the threshold and baseline for EWL projection.

V. ADDITIONAL SITES AND GLOBAL ANALYSIS

The detail of San Diego SLV results validated efficacy of the methodology and highlighted the diversity of characteristics that can be found in the proposed analysis, consequently, implementation of the methodology at different location was required to determine its accuracy. Apra Harbor, Guam, and Key West, FL, were selected to conduct a SLV analysis that can further reveal common characteristics and impacts of the methos applied as there are naval installations in those areas; however, interpretation of the results requires some level of familiarity with the environmental characteristics of each location that are not covered in this study. Detailed visualization was minimized in this chapter and in some cases only description of results was included. Once the method was proved accurate at different coastal locations, a global analysis was conducted to depict large patterns of SLV.

A. GUAM SLV ANALYSIS

Testing of the SWL and SSHA analysis methodology was performed for the Apra Harbor, Guam, tide gauge station 1631428 located at 13° 25.7′ N, 144° 47.8′ E, with the corresponding SSHA grid point (also referred as GUAM) centered at 13° 45.0′ N, 143° 45.0′ E. Guam is in a region where high seismic activity reported (such as the earthquake in 2009), which could cause an increase on sea level trends via rapid post-seismic land subsidence. It is under ECU 4, characterized by sloping with 97.87% average slope, sinuous, high erodibility, tropical moist, moderate river discharge, moderate wave energy with average significant wave height of 0.7 m, moderately tidal with average tidal range of 2.48 m, euhaline-oxic-warm to very warm, moderately turbid with average turbidity of $0.24 m^{-1}$, low chlorophyll.

1. Key Indicators

Review of hourly detrended water levels for Apra Harbor station revealed that the SWL timeseries range is 1558 mm (-927 mm in January 2019 to 631 mm in June 2008); the tidal components range is 1257 mm (-792 mm in December 2008 to 465 mm in July 2009); non-tidal components range is 953 mm (-459 mm to 494 mm in December 2002),

304 mm smaller than the tidal range. The five-day detrended GUAM SSHA, revealed a 462 mm water level range (-278 mm in August 2015 to 184 mm in December 2008). Interestingly, the highest SWL recorded happened in the 2000–2010 decade.

Comparison of the 30 largest levels for SWL, tidal and non-tidal component, showed that 10 maximum tidal events were aligned with SWL maximum events, and 10 maximum non-tidal events aligned to maximum SLW. The largest tidal events show 28 days, semiannual and interannual periodicity; and the non-tidal events are mainly accumulated over 2008–2009, and 2012–2013. For the GUAM area, the 10 largest levels are accumulated over 2008–2009, indicating agreement in magnitude and occurrence with the residual timeseries. The water level time series indicate that a combination of tidal and non-tidal water levels is what propels variability the study area as it is suspected that forcing of 2008 largest SWL event is a combination of a high tide and residual influences. Sea level trend was calculated for Apra Harbor at 3.91 mm year^{-1} based on data from October 1992 to December 2019; and for GUAM at 3.54 mm year^{-1}. The NOAA CO-OPS (NOAA Tides and Currents 2022) Apra Harbor relative sea level trend is 2.41 mm year^{-1} based on monthly sea level data from 1948–2009. These trends highlight a substantial post-seismic accelerating rise rate.

The Apra Harbor seasonality range is 110 mm (- 39 mm in December to 70 mm in July), which is composed of a tidal seasonality range of 138 mm (- 68 mm in December to 70 mm in July) added to the non-tidal seasons range of 22 mm (-8 mm to 13 mm with multiple oscillations peaking in March and dipping in October and January). The altimetry seasonality has a range of 112 mm (- 57 mm in December to 54 mm in July). There is good agreement on magnitude and timing for water levels seasonality, with most of the contribution matching SA and SSA tidal fits.

2. Non-tidal Components

Further evaluation of the residual SLW component and SSHA led to measurement of 5 non-tidal events with good agreement for the two locations (Figure 16). Figure 16a shows the detrended, residual component of Pago Pago SWL with seasoned removed, including the 30 largest water level events (grey lines) to visually contrast individual

contributions. Figure 16b shows the detrended, de-seasoned GUAM SSHA, including the 10 largest water level events (grey lines). Figure 16c shows Apra Harbor transient events with a range of 952 mm (-285 mm to 667 mm) with the maximum value recorded in December 2002 matching the passage of super typhoon Pongsona. GUAM transient filter is negligible due to temporal resolution and was not further analyzed (Figure 16d). Figures 16e and 16f, show the S2S component of water levels, for Pago Pago, and GUAM respectively. Pago Pago S2S range is 291 mm (-171 mm to 120 mm) with the maximum value recorded in February 1999; and GUAM has a range of 184 mm (-107 mm to 77 mm) with the maximum value recorded in May 2003.

Figure 16g shows Apra Harbor S2A events with a range of 197 mm (-91 mm to 105 mm) with the maximum value recorded in March 1999. For GUAM (Figure 15.h), S2A events have a 166 mm range (-87 mm to 78 mm) with the maximum value recorded in April 1997.

Figures 16i and 16j, show the IA component of water levels, for Apra Harbor, and GUAM respectively. Apra Harbor IA range is 304 mm (-194 mm to 110 mm) with the maximum value recorded in November 2008; and GUAM has a range of 302 mm (-188 mm to 114 mm) with the maximum value recorded in April 1997. Figure 16k shows Apra Harbor decadal events with a range of 57 mm (-33 mm to 24 mm with the maximum value recorded in April 2009. For GUAM (Figure 16l), decadal events have a 63 mm range (-32 mm to 31 mm) with the maximum value recorded June 2009. The close match of magnitude and patterns for IA and decadal events is interesting and demonstrates the efficacy of the filtering method used to extract the individual time series.

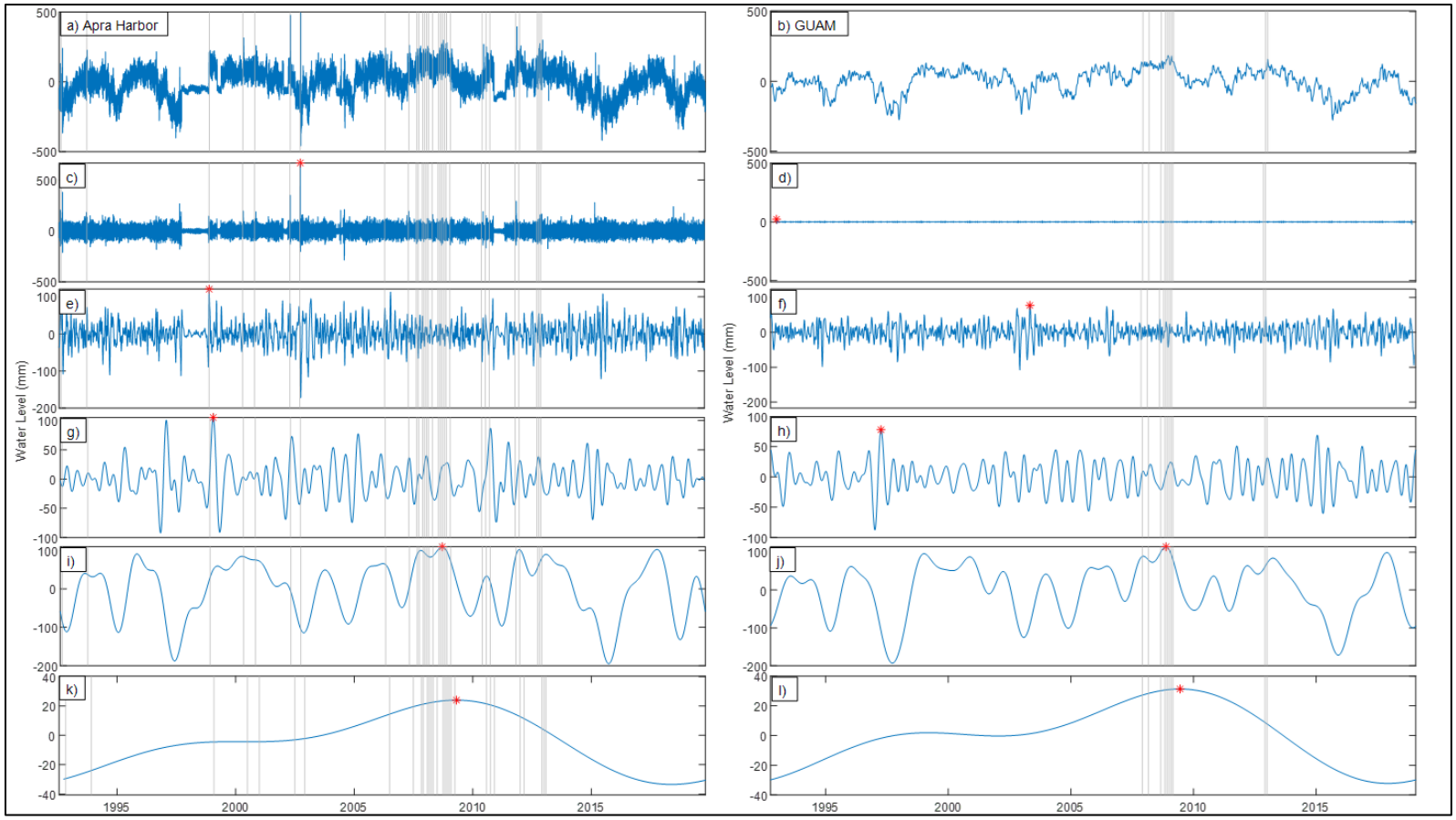

Filtered non-tidal components of detrended, de-seasoned a) Apra Harbor η_{Res}, and b) GUAM $\eta_{a,}$ time series represented by transient (c and d), S2S (e and f), S2A (g and h), IA (i and j), and decadal (k and l) events, respectively. Maximum Seal Level recorded (red asterisk). SWL residual 30 largest events and SSHA 10 largest events depicted (gray lines).

Figure 16. Guam Non-tidal Component Filters

3. SLV Contributors

The "thumbprint" of the interaction and contribution of Apra Harbor SWL components is presented in Figure 17, with a 432 mm SWL 99th percentile; a 345 mm tidal 98th percentile; and a 177 mm residual 99th percentile. There were no instances when the water level from the combined components was above734 mm, exceeding the SWL 99th percentile by at least one foot; however, variability was significant (up to 724 mm) below the residual 1st percentile (-254 mm), exceeding up to 1 foot below. IA events are noticeable throughout the time series. Aligned with California results, S2S phenomena is consistently the prevailing variability driver by either constructive or destructive interference as it propels water level patterns.

4. Maximum Water Levels

Extremes of SLV for the Guam area recorded from 1992 to 2019 are shown in Figure 18. Apra Harbor SWL extreme scenario has maximum water levels ranging from 831 mm at its lowest in March to 1279 mm in December at its highest (Figure 18a). Tides had a low variability (136 mm) ranging from 327 mm in December to 462 mm in July; transient events have the largest variability (518 mm) ranging from 146 mm in May to 664 mm in December; S2S variability is between 71 and 120 mm; S2A is between 42 and 103 mm; IA from 85 to 107 mm; decadal maximum contribution is 28 mm throughout the year. Figure 18b depicts Apra Harbor non-tidal and seasonal combined contribution ranging from 446 mm in April to 951 mm in December.

Figure 18.c shows GUAM EWL range from 248 mm at its lowest in March to 287 mm in July at its highest; IA events have the largest variability ranging from 67 mm in April to 98 mm in October; S2S variability is between 24 and 44 mm being lowest in January and largest in July; S2A variability is between 84 and 114 mm being lowest in April and largest in November; and decadal maximum contribution is 31 mm throughout the year.

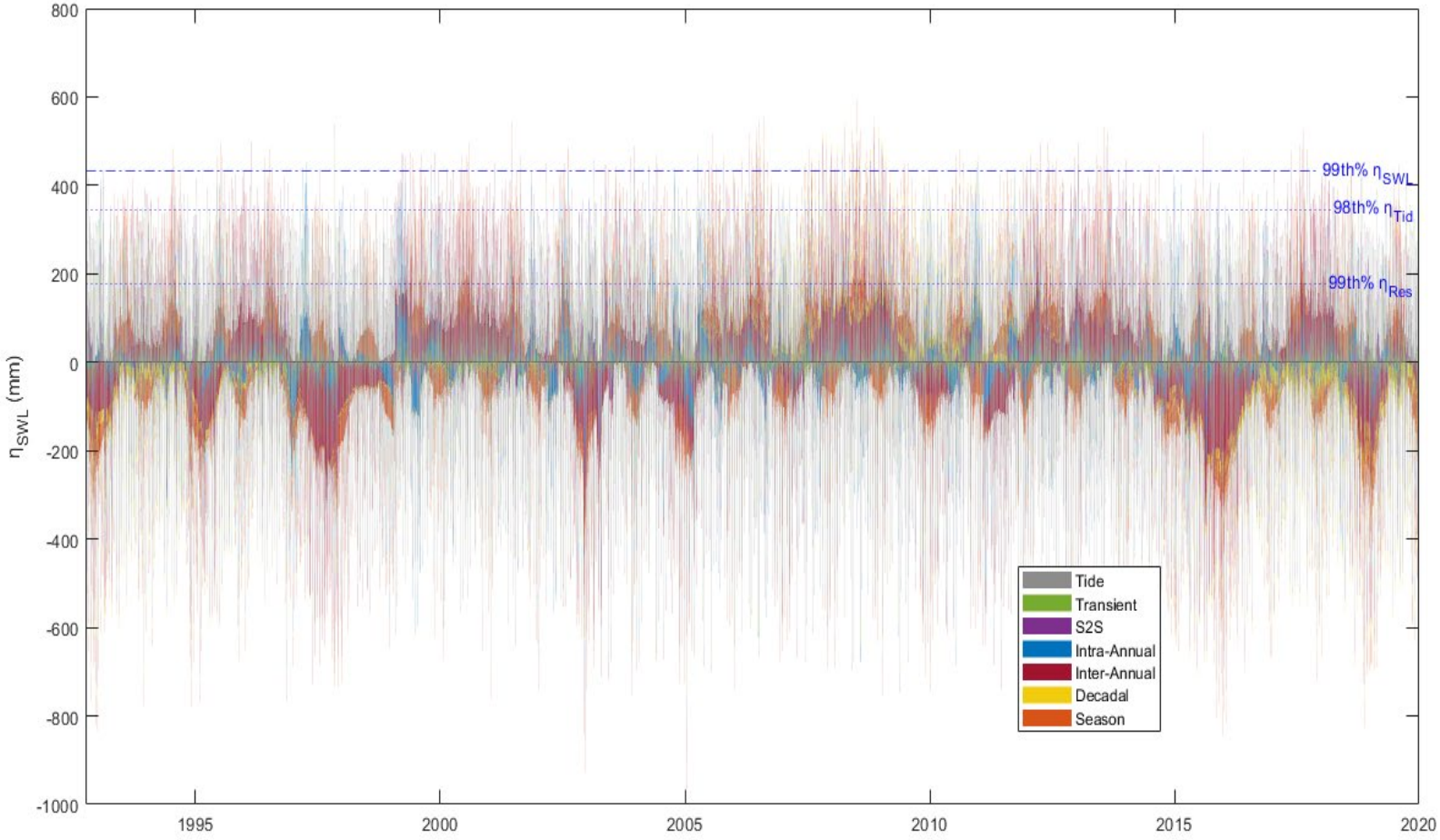

SWL "thumbprints" unique to a) Apra Harbor represented in a fishbone of compiled contributors from 1992 to 2019. SWL 99th %, tides 98th %, and residual 99th % (blue dash lines) noted.

Figure 17. Apra Harbor SWL Stacked Contributors

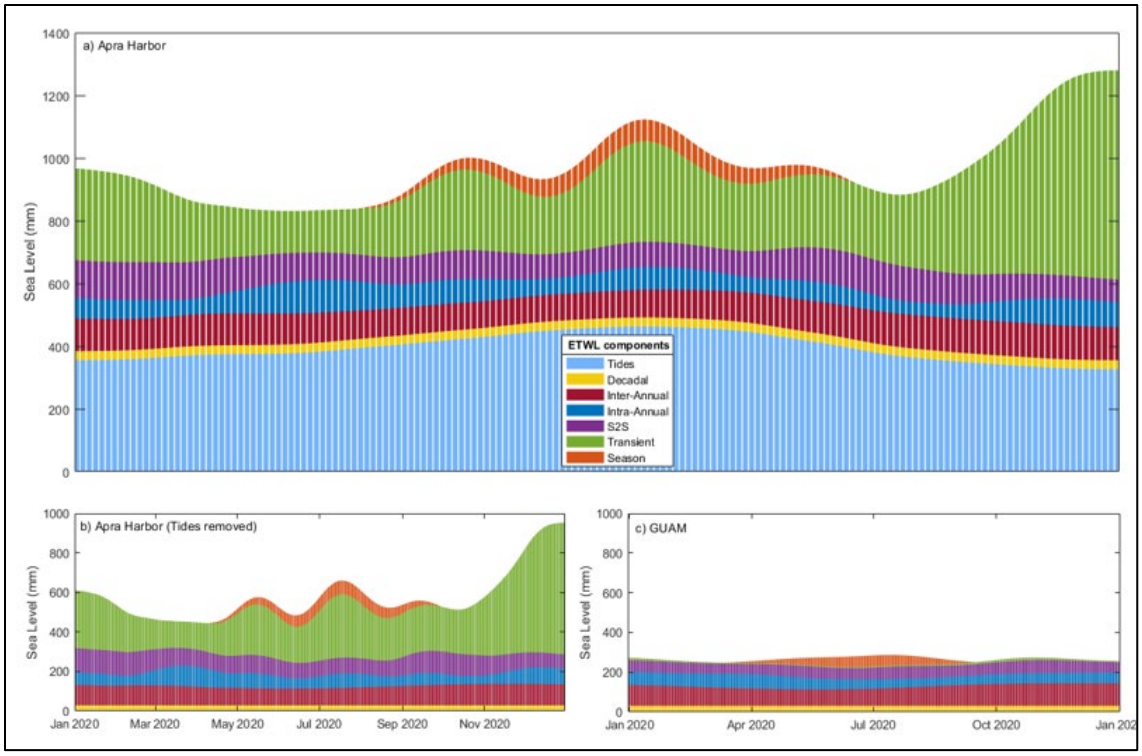

Maximum sea level for a) Apra Harbor, b) Apra Harbor (tides removed), and c) GUAM, in a year are represented by color-coded combination of factors using levels recorded from 1992 to 2019

Figure 18. Guam Sea Level EWL Components

5. Climate-Driven SLV

Figure 19 shows the κ value for the Guam area SSHA related to climate indices. The 95% significance levels are $\kappa_{95\%} \sim 0.38$, and any correlation not meeting this significance falls below the red dashed line. Guam shows the largest statistically significant of SSHA to the Niño 3.4, Niño 4, MJO 4, MJO 8, and MJO 9 ($\kappa > 0.44$); and significant response to MJO2 and MJO3 ($\kappa \sim 0.40$). Responses to the ENSO indices was an expected result for Pacific coastal locations since ENSO predominantly impacts the ocean circulation in the equatorial Pacific region. The high coherence between SSHA (143°E) and the MJO 4 (140°E) is potentially due to perturbations interference between the ENSO and the expected MJO cyclic pattern in that region.

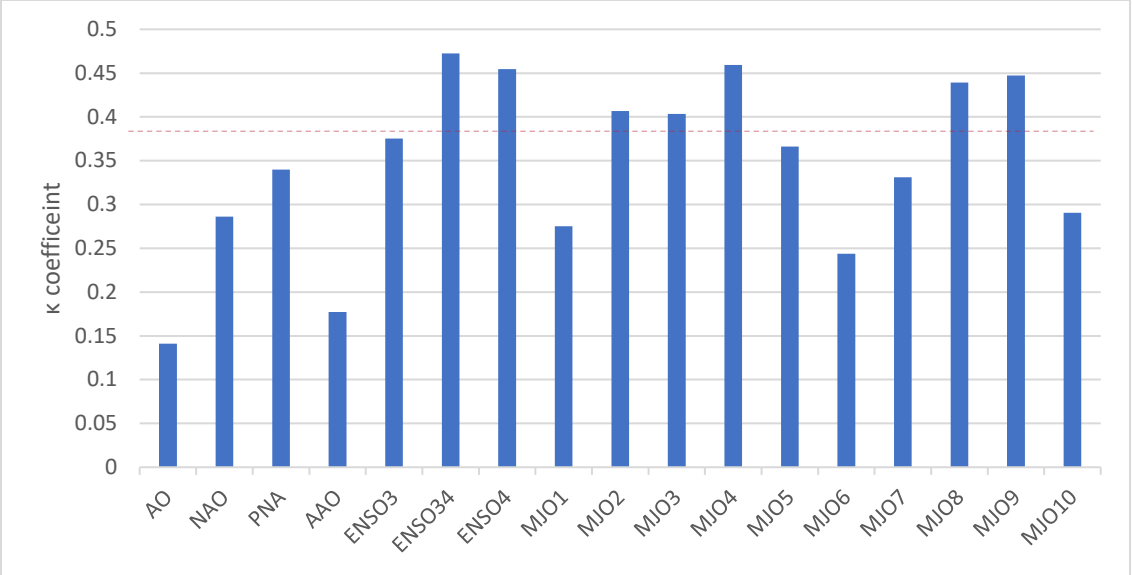

κ between water levels and daily climate indices. The proportion of the standard deviation of GUAM sea level accounted for by the AAO, the AO, the NAO, the PNA, the ENSO, and MJO is represented by κ. The 95% significance levels are $\kappa_{95\%} \sim 0.38$ (red dashed line).

Figure 19. GUAM SLV Relationship to Climate Modes

B. KEY WEST, FLORIDA, SLV ANALYSIS

Testing of the SWL and SSHA analysis methodology was performed for Key West, Florida, tide gauge station 8724580 located at 24° 33.0′ N, 81° 48.5′ W, with corresponding SSHA grid point centered at 23° 75.0′ N, 82° 45.0′ W from 02 October 1992 to 31 December 2019.

1. Key Indicators

Hourly detrended water levels for Key West station revealed that the SWL timeseries range is 1639 mm (-627 mm to 1012 mm); the tidal components range is 1036 mm (-487 mm in to 549 mm); non-tidal components range is 1175 mm (-352 mm to 823 mm), 163 mm larger than the tidal range and with both extremes occurring on the same day (24 October 2005). The five-day detrended South Florida SSHA, revealed a 286 mm water level range (-128 mm to 158). Interestingly, the largest SWL events are mainly maximum non-tidal events, an indication that transient events are the largest SVL driver at this location.

Sea level trend was calculated for Key West at 2.57 mm per year based on data from October 1992 to December 2019; and for South Florida at 3.61 mm per year. The NOAA CO-OPS (NOAA Tides and Currents 2022) Key West relative sea level trend is 2.52 mm per year based on monthly sea level data from 1913 to 2021. Even though the range over which the SWL rate is calculated is different, the SWL trend magnitudes are almost identical; indicating a large difference between SWL and altimetry that can only be explained by transient events as the substantial sea level change rate for altimetry only captures lower frequencies.

Key West seasonality range is 245 mm (-96 mm in February to 147 mm in October), composed by a tidal seasonality range of 228 mm (-99 mm in to 129 mm) added to the non-tidal seasons range of 40 mm (-21 mm to 19 mm). The altimetry seasonality range is 109 mm (-48 mm to 60 mm) with good alignment in occurrence with SWL, with majority of the seasonal contribution matching annual and semiannual tidal fits.

2. Non-tidal Components

Filtered non-tidal components of detrended, de-seasoned residual and SSHA timeseries are shown in Figure 20. Figure 20a shows the detrended, seasons removed residual component of Key West SWL, including the 30 largest water level events (grey lines) to visually contrast individual contributions. Figure 20b shows the detrended, seasons removed South Florida SSHA, including the 10 largest water level events (grey lines). Figure 20c shows Key West transient events with a range of 1139 mm (-309 mm to 830 mm) with the maximum value recorded in October 2005. South Florida transient filter is negligible due to temporal resolution and was not further analyzed (Figure 20d). Figures 20e and 20f, show the S2S component of water levels, for Key West (291 mm range with the maximum value recorded in June 2012), and South Florida (163 mm range with the maximum value recorded in January 2017). Figures 20g and 20h, show the IA component of water levels, for Key West (195 mm range with the maximum value recorded in February 1999), and South Florida (131 mm range with the maximum value recorded in December 2015). Figures 20i and 20j, show the decadal component of water levels, for Key West (21 mm range with the maximum value recorded in 2018), and South Florida (27 mm range with the maximum value recorded in 2017). These results corroborate that transient phenomena is the predominant water level driver at Key West.

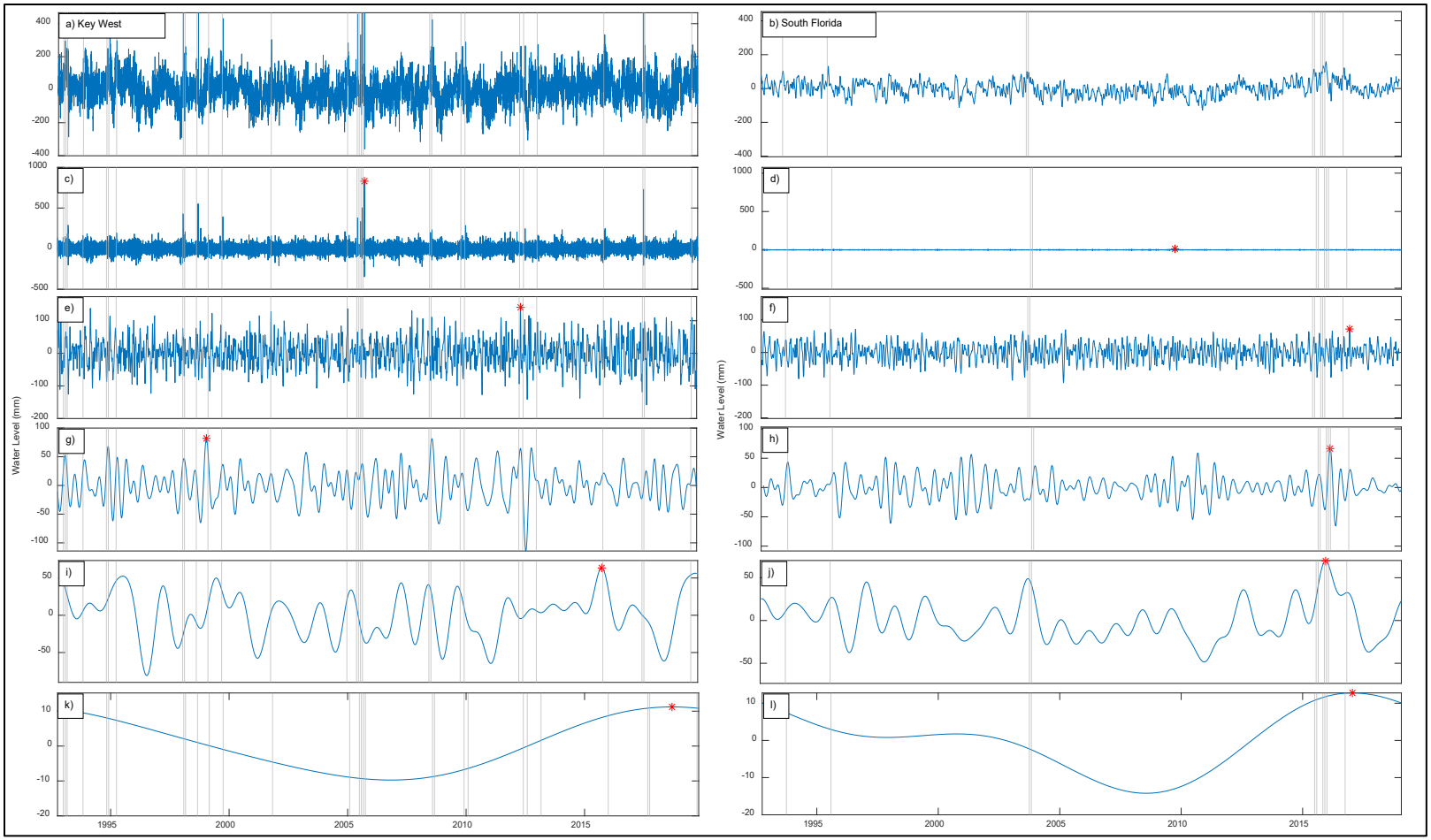

Filtered non-tidal components of detrended, de-seasoned a) Key West η_{Res}, and b) South Florida η_a, time series represented by transient (c and d), S2S (e and f), S2A (g and h), IA (i and j), and decadal (k, and l) events, respectively. Maximum Seal Level recorded (red asterisk). SWL residual 30 largest events and SSHA 10 largest events depicted (gray lines).

Figure 20. Florida Non-tidal Component Filters

3. SLV Contributors

The "thumbprint" of the interaction and contribution of Key West SWL components is presented in Figure 21, with a 442 mm SWL 99th percentile; a 358 mm tidal 98th percentile; and a 183 mm residual 99th percentile. There were four instances when the water level from combined components was above746 mm, exceeding the SWL 99th percentile by at least one foot. The largest events match the occurrence of Hurricane Georges (25 September 1998), Hurricane Wilma (25 October 2005) and Hurricane Irma (10 September 2017). Detailed inspection of the compiled water levels revealed the transient component, followed by the seasonal and the IA component impact sea levels in Key West; however, S2S phenomena is consistently the prevailing variability driver by either constructive or destructive interference as it propels water level patterns.

4. Maximum Water Levels

Extremes of SLV for the South Florida area recorded from 1992 to 2019 are shown in Figure 22. Figure 22a shows Key West SWL extreme scenario with the maximum water levels range from 796 mm at its lowest in May to 1713 mm in October at its highest; tides have low variability (211 mm) ranging from 332 mm in March to 543 mm in October; transient events have the largest variability (604 mm) ranging from 133 mm in May to 794 mm in October; S2S variability is between 113 and 132 mm; S2A variability is between 41 and 80 mm; IA from 43 to 64 mm; decadal maximum contribution is 11 mm throughout the year. Figure 22b depicts Key West non- tidal and seasonal combined contribution ranging from 380 mm in to 951 mm (793 mm). Figure 22c shows South Florida EWL range from 169 mm to 260 mm with the order of magnitude and patterns align SWL.

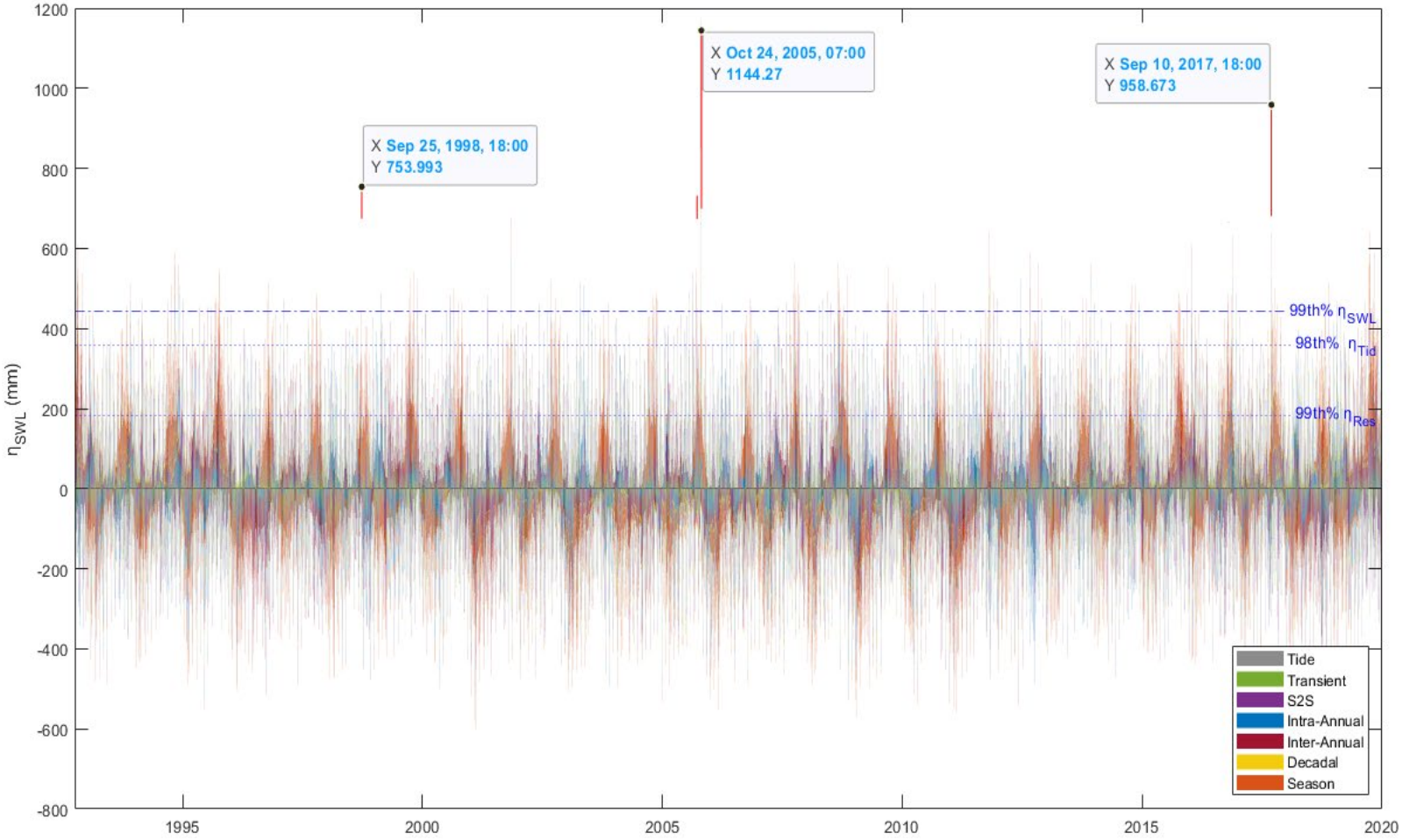

SWL "thumbprints" unique to a) Key West represented in a fishbone of compiled contributors from 1992 to 2019. SWL 99th %, tides 98th %, and residual 99th % (blue dash lines) noted.

Figure 21. Key West SWL Stacked Contributors

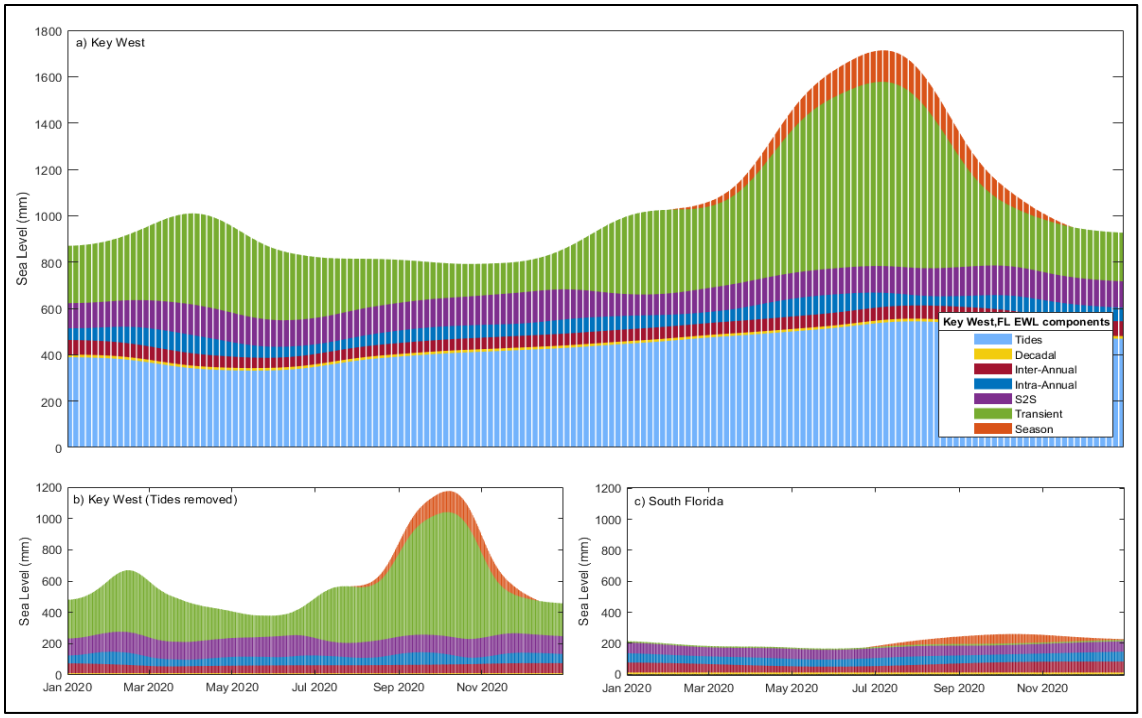

Maximum sea level for a) Key West, b) Key West (tides removed), and c) South Florida, in a year are represented by color-coded combination of factors using levels recorded from 1992 to 2019.

Figure 22. Key West Sea Level EWL Components

5. Climate-Driven SLV

Figure 23 shows the κ value for Key West area SSHA related to climate indices. The 95% significance levels are $\kappa_{95\%} \sim 0.38$, and any correlation not meeting this significance falls below the red dashed line. Key West shows the largest statistically significant response of SSHA to the NAO ($\kappa \sim 0.496$); and significant response to ENSO 3.4, MJO 2, MJO 3, MJO 7, and MJO 8 (κ~0.38 to 0.42). Relation to the NAO indices is an expected result for North Atlantic coastal locations. The coherence of SSHA to the MJO is potentially due to the perturbations in the regional low-level moisture availability and upper-tropospheric flow leading to pressure pattern changes in the Southeast U.S. (Arcodia et al. 2020).

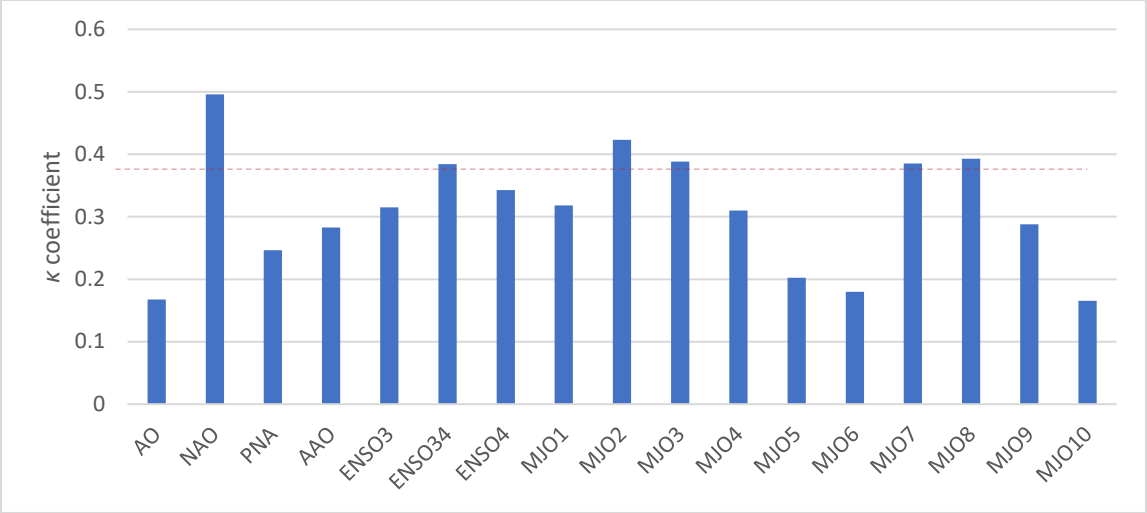

κ between water levels and daily climate indices. The proportion of the standard deviation of Key West sea level accounted for by the AAO, the AO, the NAO, the PNA, the ENSO, and MJO is represented by κ. The 95% significance levels are $\kappa_{95\%} \sim 0.38$ (red dashed line).

Figure 23. Key West SLV Relationship to Climate Modes

C. GLOBAL SLV ANALYSIS

The success of the methodology using tide gauge and altimetry data for coastal areas motivated a further effort of expansion to understand regional SLV at any given location, therefore, the proposed methodology was replicated to assess SLV for the entire SSHA dataset. This was done because tide gauge data has not been collected at many locations, so a space-based estimate of SLV provides an estimate of regional variability for such locations that can be used as a starting point for quantifying the effects of various drivers of sea level even in the absence of gauge data. It is noted that degrading the spatial resolution of the dataset limits coastal analysis and further coastal SLV analysis requires in situ measurement as proved in previous sections. Global analysis using altimetry is important as it provides a larger level of understanding of open ocean SLV and the coupled lower frequency ocean-atmospheric processes exciting sea level patterns. The spatiotemporal resolution tradeoff that complemented tide gauge analysis, turns into an advantage as tidal and high frequency complexities are removed, allowing for depiction of offshore forcing.

1. Global Maximum Water Levels

Analysis of individual contributors to SSHA was repeated using the sum of individual contributors' maxima per grid point for the period events from 1992 to 2019, producing a global map of maximum sea level anomaly with all contributors combined (Figure 24). The variability seen in the East equatorial Pacific, northeast Atlantic, south of Africa, east of South America, east of Japan, and in vicinity to the Maritime Continent, reaches magnitudes up to 937 mm and show particularly interesting patterns, with some resemblance to the warm ocean circulation that could be a product of combined short-term effects of storm-induced variability, sterodynamic changes and water masses heterogeneity.

In terms of temporal resolution, separating out the processes gives the impression that variability in the Northern Hemisphere storm tracks is due to combination of multiple contributors' variability when the poor temporal resolution of the data (5-day) is causing observed transient events that cannot be filtered out to get aliased onto lower frequency variability. For example, transient events are defined as those with periodicity of less than 15 days. However, the altimeter dataset is created as a blend of altimeter data over a 5-day period. If a storm passes over a particular area when the altimeter observes that area, then it may have an exaggerated contribution to the altimeter SSHA estimate for that 5-day period. Furthermore, when trying to filter for phenomena related to S2S variability with periods of less than 100 days, one or two extreme events occurring within a 100-day period, which encompasses just 20 points of altimeter data, could result in erroneously projecting onto the S2S (or even IA) time series. Because of this, separating non-tidal components on a global scale is meaningless, and only the maximum of the sum of all contributors is shown in Figure 24.

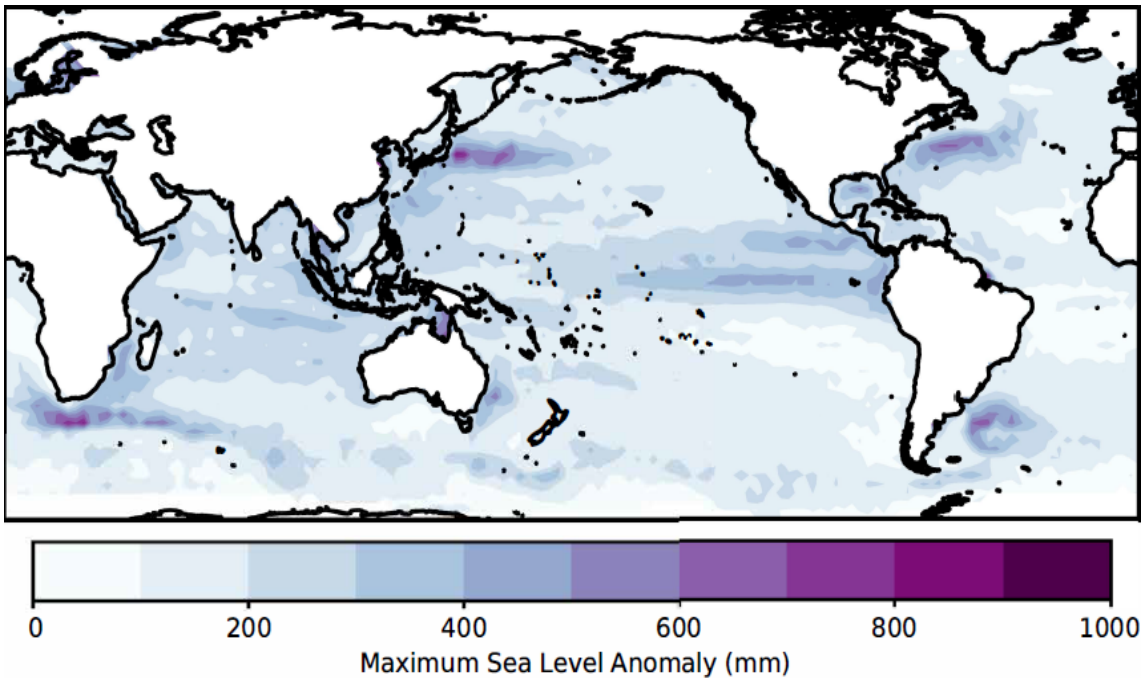

EWL representation. Global map of the contributors' maxima sum per grid point from 1992 to 2019.

Figure 24. Global Maximum Sea Level Anomaly

2. SLV Atmospheric Teleconnections

Global response of sea level to different climate modes is presented in this section. Figure 25 shows global maps of κ for the SSHA related to circulation modes AAO, AO, NAO, and PNA. The 95% significance levels are $\kappa_{95\%} \sim 0.38$; orange dots in each panel indicate where κ is statistically significant. Figure 25a is the map of the amount of SLV related to the AAO; where the oceans show a statistically significant response (maximum κ is 0.41) of sea level to the AAO around the poles, west and south of Australia, at coastal areas on the eastern North Atlantic Ocean, Brazil basin, mid latitude spots in the Northeast Pacific basin, Mascarene basin in vicinity to Madagascar, and Mid-Indian Basin. The weak and random relation could be due to length of AAO positive and negative patterns being shorter than 15 days and it is not captured by altimetry, or by the random length between positive and negative patterns that can interfere with other significant forcing signals. Figure 25b is the map of the amount of SLV related to the AO; where the oceans show a statistically significant response (maximum κ is 0.4) of sea level to the AO is minimal and

random at latitudes close the poles, and near the Tiki basin in the South Pacific Ocean. As with the AAO, weak and random response could be due to length of patterns, or to poor understanding of direct impacts of polar sea level pressure anomaly interfere in water levels; or it could be that the AAO and AO simply do not impact sea level in a direct way other than impacting sea-ice extent by advection of warm air driving ice northward (or southward) when there are anomalous surface winds.

Figure 25c is the map of the amount of SLV related to the NAO; where the oceans show a statistically significant response (maximum κ is 0.72) of sea level to the NAO at coastal areas in the North Atlantic Ocean, The Mediterranean Sea, the Arabian basin, the Red Sea, eastern basins of the Pacific Ocean, the Gulf of California, and the Northeast Pacific Basin. This is consistent with the NAO influence on mesoscale, synoptic, and global scale circulations in the northern extratropical regions, especially extratropical cyclone activity. Figure 25d is the map of the amount of SLV related to the PNA; where the oceans show an intermediate statistically significant response (maximum κ is 0.51) of sea level to the PNA along the Equator, coastal areas of the North Pacific Ocean, near the South Pacific basin, and Maritime continent. This coherence is likely due to the low frequency IA variability being influenced by the ENSO.

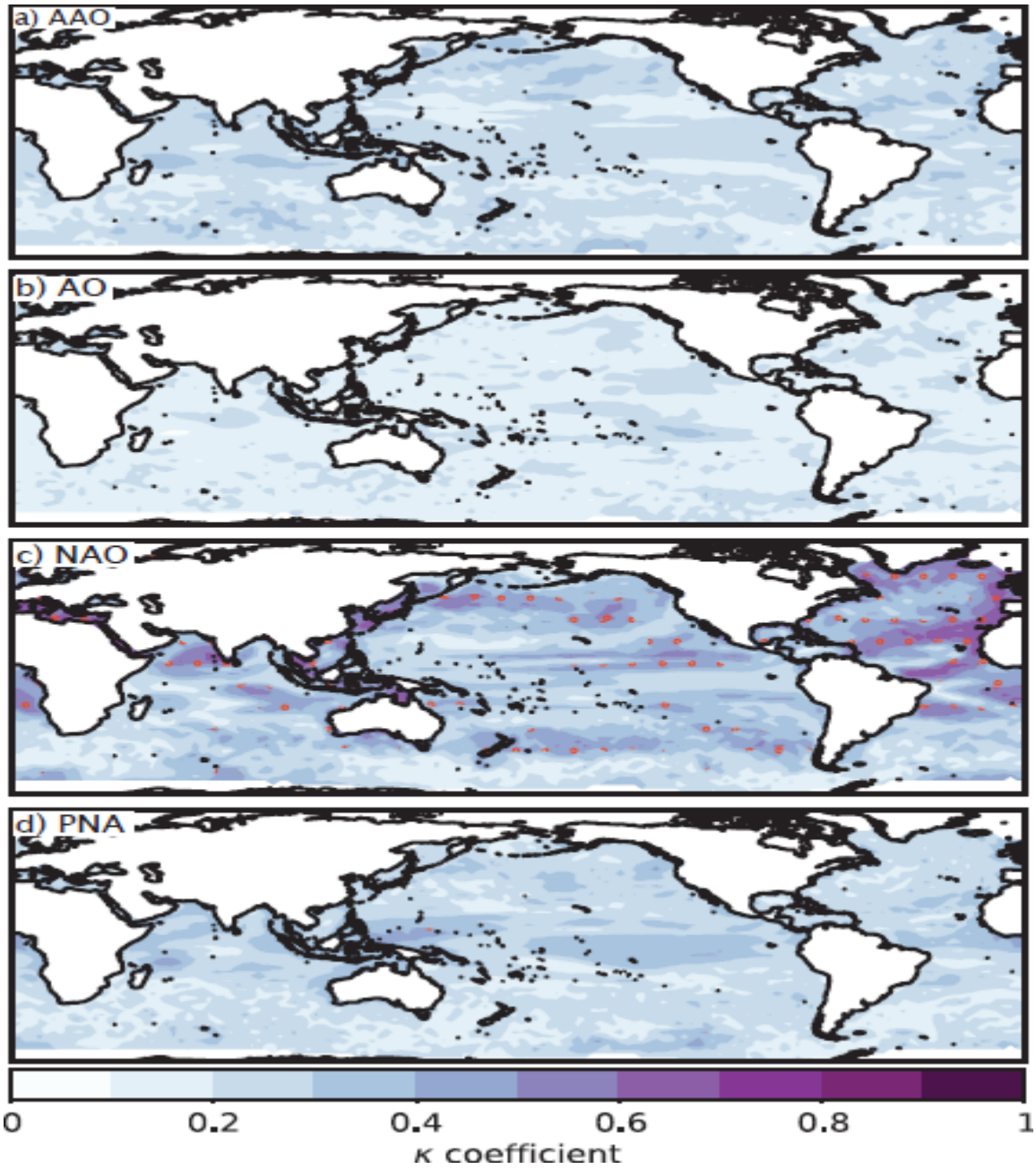

Worldwide maps of the amount of global SLV related to Circulation Climate Indices. a) The proportion of the standard deviation of sea level accounted for by the a) AAO, b) the AO, c) the NAO, and d) the PNA, is represented by κ. The 95% significance level is $\kappa_{95\%} \sim 0.38$.

Figure 25. SLV Relationship to Circulation Modes

Figure 26 shows global maps of the κ value for the SSHA related to the ENSO. The 95% significance levels are $\kappa_{95\%} \sim 0.38$. Figures 26a, 26b, and 26c are the maps of the amount of SLV related to the ENSO 3 (maximum k is 0.82), ENSO 4 (maximum κ is 0.77), and ENSO 3.4 (maximum κ is 0.84) respectively, where the oceans show a statistically significant coherence of sea level to the ENSO around the Equator and coastal regions in the easter Pacific Ocean. This is consistent with the complex tropical ocean and atmosphere variations patterns of ENSO (Han et al. 2019) and an expected result that gives validity to the methods.

Figure 27 shows global maps of the κ value for the SSHA related to the MJO. The proportion of the standard deviation of sea level accounted for by the MJO1 (Figure 27a), the MJO2 (Figure 27b), MJO3 (Figure 27c), the MJO4 (Figure 27d), MJO5 (Figure 27e), the MJO6 (Figure 27f), the MJO7 (Figure 27g), the MJO8 (Figure 27h), the MJO9 (Figure 27i), and the MJO 10 (Figure 27j), is represented by κ. For all the MJO patterns, an evident significant coherence is in the Equatorial Pacific, reaching to the Maritime Continent coastal regions on the Pacific Ocean side. The weakest response is to the MJO 6 (maximum κ is 0.55). This may imply that the strongest coherence between SSHA and MJO happens because of processes that occurred when the MJO-related convective anomalies (either positive or negative) were propagating through the Maritime Continent and are not so dependent upon the upward or downward branches of the MJO circulation passing through the East Pacific.

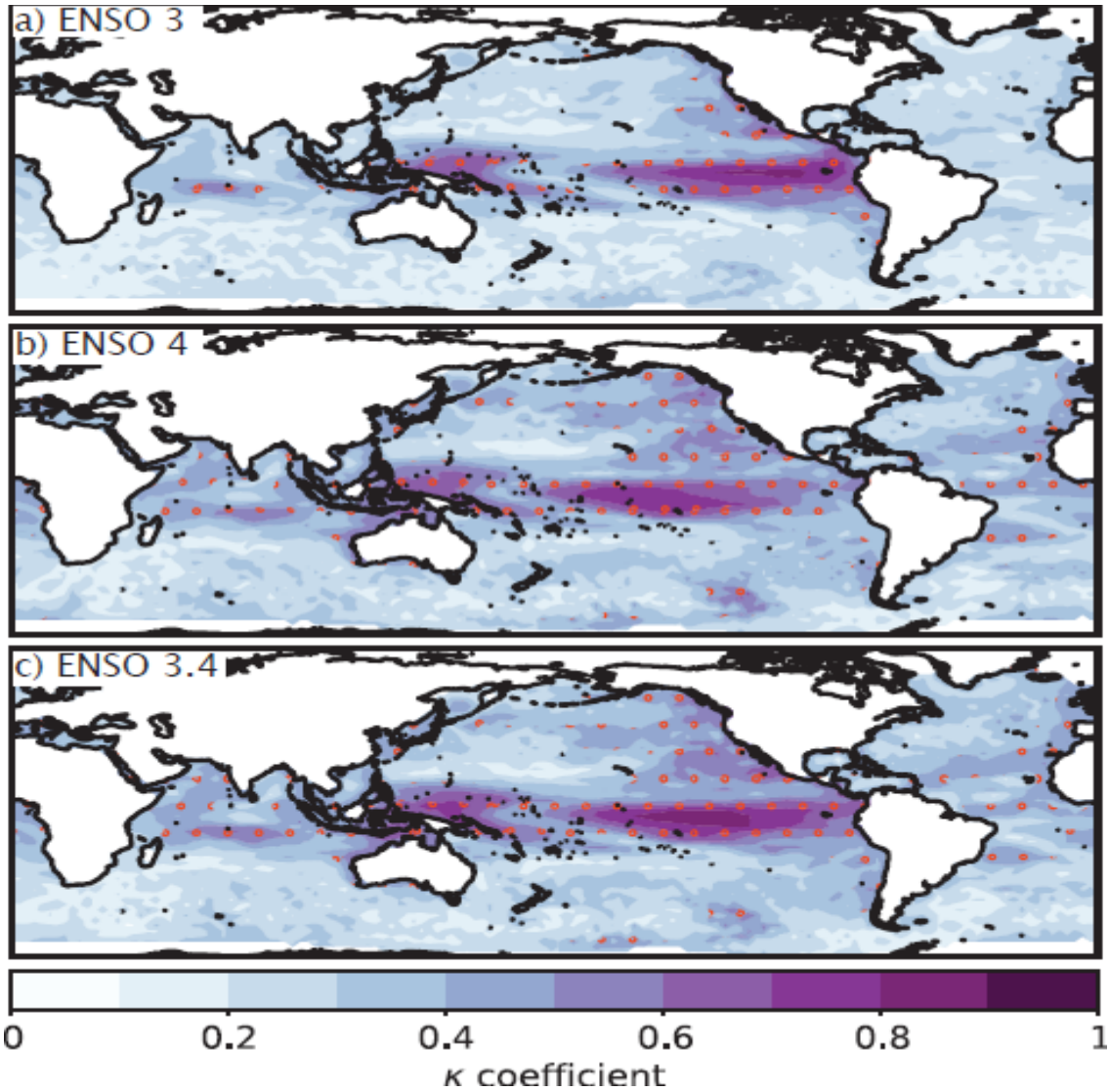

Worldwide maps of the amount of global SLV related to ENSO Indices. a) The proportion of the standard deviation of sea level accounted for by the a) Niño 3, b) the Niño 4, and c) the Niño 3.4, is represented by κ. The 95% significance level is $\kappa_{95\%} \sim 0.38$

Figure 26. SLV Relationship to ENSO

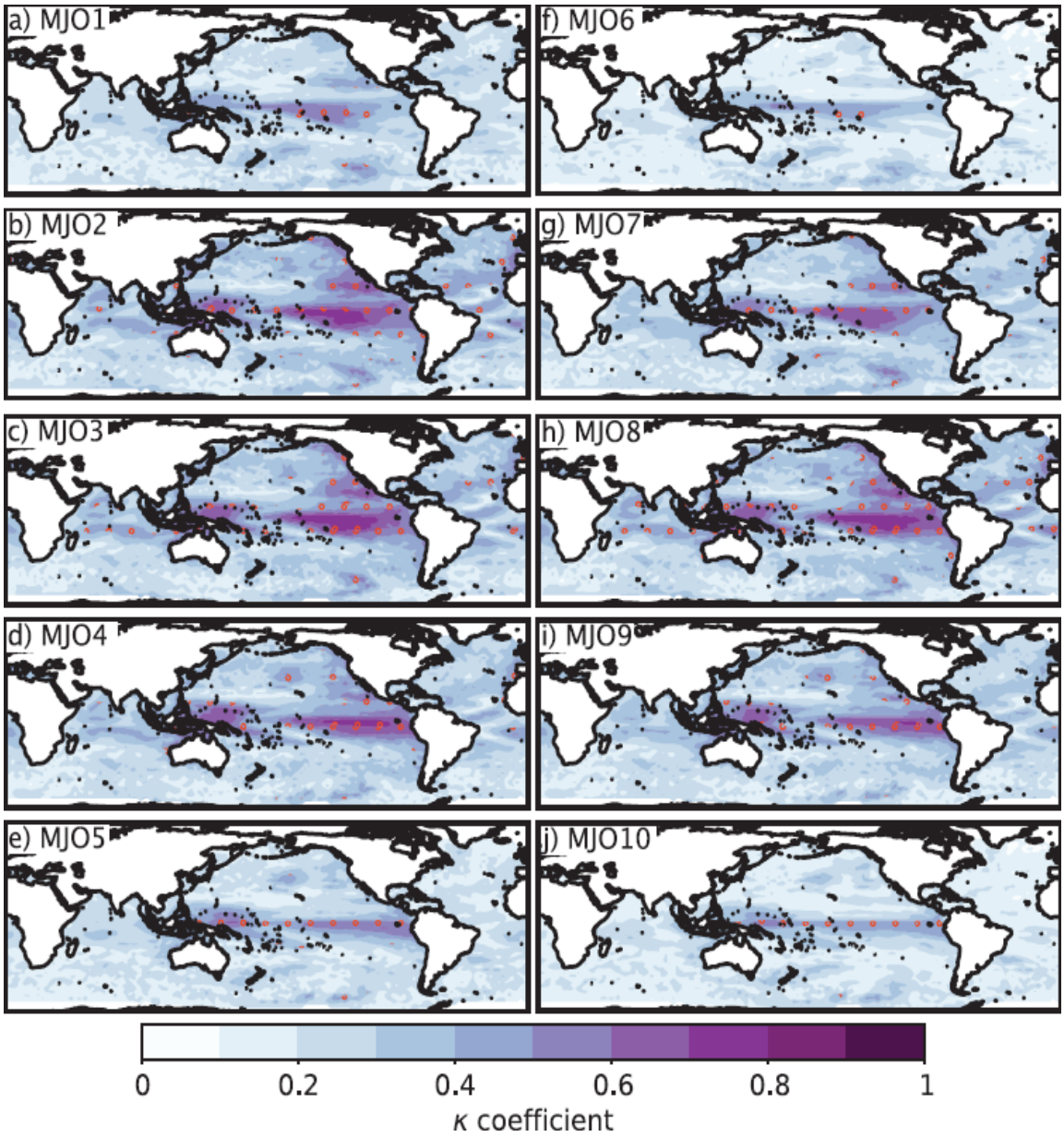

Worldwide maps of the amount of global SLV related to the MJO. The proportion of the standard deviation of sea level accounted for by the a) MJO1, b) the MJO2, c) MJO3, d) the MJO4, e) MJO5, f) the MJO6, g) MJO7, h) MJO8, i) the MJO9, and j) the MJO 10, is represented by κ. The 95% significance level is $\kappa_{95\%} \sim 0.38$

Figure 27. SLV Relationship to MJO

D. SUMMARY

Contrasted to San Diego, Guam findings present lower SLV that become minimal at lower frequencies. Although transient processes are of large range and tropical storms (i.e., Typhoon Pongsona 2002) are the core of EWL in that area, IA variability (mainly ENSO) is a key driver. The comparison between altimetry versus gauge data, revealed very similar patterns with an exact match in orders of magnitude for deep ocean and coastal water levels as frequency decreases, an unanticipated finding as seismic activity is expected to impact LVM and low frequency processes. The analysis at Key West, identified the scenario of a location susceptible to SLV from transient events (tropical storms), where the extremes are lower in occurrence, but the magnitude surpasses thresholds (hurricanes); and S2S contributions are the second largest SLV driver (mainly NAO). A significant finding common to the three study areas was that out of all SLV contributors, only the patterns of S2S processes are always of constructive interference (and all site showed some relation to the MJO). A significant difference between the additional sites and San Diego is the unremarkable influence of tides in maximum water levels.

From the global analysis, it is interesting, for the first time, to map the global sea level maxima and global ocean response of the sea level to climate variability modes (with exception of the MJO by Oliver and Thompson in 2010), recognizing that the analysis can only denote S2S or lower frequencies variability owing tidal and coastal processes complexities are removed. These representations indicate that variability of climate modes is not only in low frequencies; some modes have phases with transient to S2S variability, therefore, the weak response of SSHA levels to AO, AAO, PNA could be explained by the poor temporal resolution of altimetry data, a notable finding, since all the modes analyzed manifest teleconnections and involve coupled ocean-atmospheric processes.

The presented findings are in striking agreement with unique characteristics and patterns observed at each location, which proves that calculation of offshore forcing water level budget at local scales with orders of magnitude of key coastal SLV drivers can be derived from altimetry and tide gauge data using the method formulated in Chapter III.

THIS PAGE INTENTIONALLY LEFT BLANK

VI. CONCLUSIONS

This study explored whether approximations of key processes driving coastal water level variability can be derived from altimetry and tide gauge data at the same or larger precision than theoretical approximations using model representation. To determine this, an objective methodology for identification and quantification of SLV components was developed. Patterns and orders of magnitudes accounting for meteorology and oceanography (METOC) factors were characterized in a spatial analysis framework to provide data-driven decision-making tools to DON and DOD planners.

This project analyzed SWL, SSHA, and climate mode indices to identify the processes that influence SLV. By identifying tidal, seasonal, and non-tidal contributions, this study provided a refined frequency-derived assessment of water levels variability with the most significant finding of S2S signal always presenting as constructive interference for any location at any point in the time series at the sites analyzed, which points to a potential effect of MJO on sea levels. The global analysis maps provided a larger level of understanding of open ocean SLV and the coupled lower frequency ocean-atmospheric processes driving sea level patterns beyond the scope of uncoupled oceanography or meteorology studies.

In terms of contribution quantification, it was found that spring tides were the primary SLV driver at San Diego with a strong contribution from IA and transient events. However, manifestation and strength of transient near-shore processes differ for semi-enclosed harbors and open beaches as defined by 40 (48) extreme events observed in San Diego (La Jolla), indicating that IA events exacerbate tidal SLV pointing to ENSO as the core climate driver for the area with some MJO influence. In Guam, transient components (mainly tropical storms), exacerbated by IA processes (ENSO) have been the SLV drivers in the area with the passage of Super-typhoon Pongsona in December 2002 as the strongest EWL recorded. For Key West, transient components in the form of tropical storms are the SLV driver in the region; there is a large influence of S2S events, pointing to NAO as the core climate driver for the area with some MJO and ENSO influence as observed by

reconstruction of the three strongest EWL events that matched the passage of hurricanes Georges (1998), Wilma (2005), and Irma (2017).

A very interesting finding in San Diego was that MJO correlation coefficients were greatest for interannual variability, rather than S2S, and conversely, for SOCAL some kappa coefficients were larger for MJO than for ENSO; a similar pattern was seen in Guam and Key West, indicting an IA (mainly ENSO) and MJO synergy; indicating that filtering is a powerful way to further analyze the MJO phenomena (or any climate mode) in order to determine the component of the oscillation impacting sea levels.

In terms of the variability timescales of teleconnection patterns, the constructive or destructive interference between the different modes is very important for understanding the influences and impacts at different locations. For the NAO, there was a significant response outside the North Atlantic basin, presumably enhanced by seasons; the low response of sea level to other circulation climate modes, is likely due to the variability they fall under (i.e., AO and AAO phases are usually 12 to 15 days long, PNA presents a random variability) combined to the altimetry low temporal resolution (every 5 days), making any transient phenomena (1-15 days) negligible.

In sum, this research concluded that detailed coastal SLV analyses are possible using SWL, as its refined temporal resolution improves the decomposition of factors and enhances understanding of offshore forcing at different frequency bands, especially for characterization of tidal, transient, and extreme events. It was found that combining standardized and complementary datasets allows for identification of forcing factors at locations where in situ observations are not available, with results limited to lower frequency variability.

The findings on the San Diego, Key West, and Guam locations, provided refined details on previous local coastal characterizations, and proved the efficacy of a methodology that can be implemented globally. The work completed here can be reproduced at any location that has properly recorded and maintained datasets. The strength of connection linking climate modes to SLV was developed using traditional statistical methods that allowed to map the SSHA relationship to atmospheric teleconnections at

global scale and enabled identification of regions across the world that have a significant connection between climate modes and sea level.

Future efforts should be towards establishing tide gauge stations at naval coastal facilities (specially OCONUS), which can be cost efficient compared to mitigation efforts or corrective actions that currently lack of data driven plans to support the outcome from local scenarios. Tide gauges temporal resolution combined with the improved spatial resolution of the latest altimeter Sentinel-6 Michael Freilich Satellite (Sentinel-6/Jason CS mission), will refine SLV analysis and can certainly enhance DOD capabilities on understanding the main environment in which naval forces conduct operations. For a deeper understanding of individual contributors' dynamics, assessments using frequency dependent EOF analysis at regional level should be performed to identify physical processes across all modes of SLV; this can lead to improvement of forecasting systems at Naval coastal installations.

THIS PAGE INTENTIONALLY LEFT BLANK

APPENDIX

Results of signal spectral analysis and probability distribution for San Diego, using magnitude squared coherence, CPSD, and κ coefficient to determine the ocean response of sea level to individual contributors or to the climate variability mode are presented in this section.

Figure 28 shows San Diego probability distribution histograms for η_{Res} (Figure 28a), η_{Tr} (Figure 28b), η_{S2S} (Figure 28c), η_{S2A} (Figure 28d), η_{IA} (Figure 28e), and η_{DC} (Figure 28f). 99th% and 1st% noted (red dash lines). Figure 29 shows San Diego SWL magnitude-square coherence (Figure 29a), and spectra (Figure 29b) with periodicity indicated by red dash lines. Figure 30 shows κ of individual contributors for San Diego (Figure 30a), and SOCAL (Figure 30b).

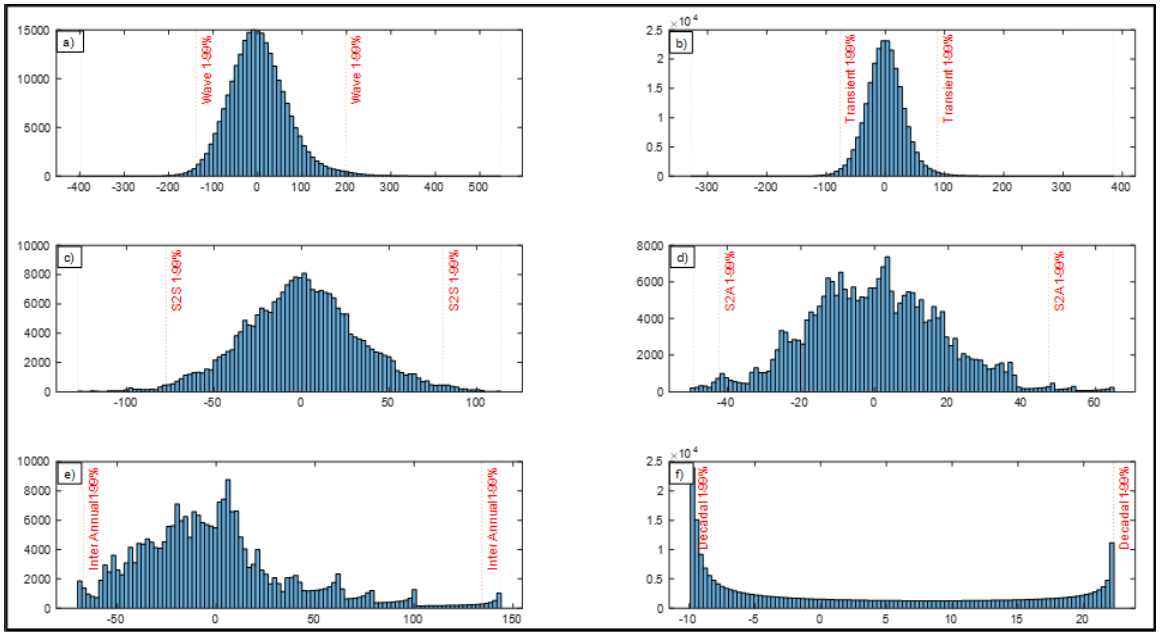

San Diego probability distribution histograms for a) η_{Res}, b) η_{Tr}, c) η_{S2S}, d) η_{S2A}, e) η_{IA}, and f) η_{DC}, calculated to validate findings. 99% and 1% noted (red dash lines).

Figure 28. San Diego Residual Distribution

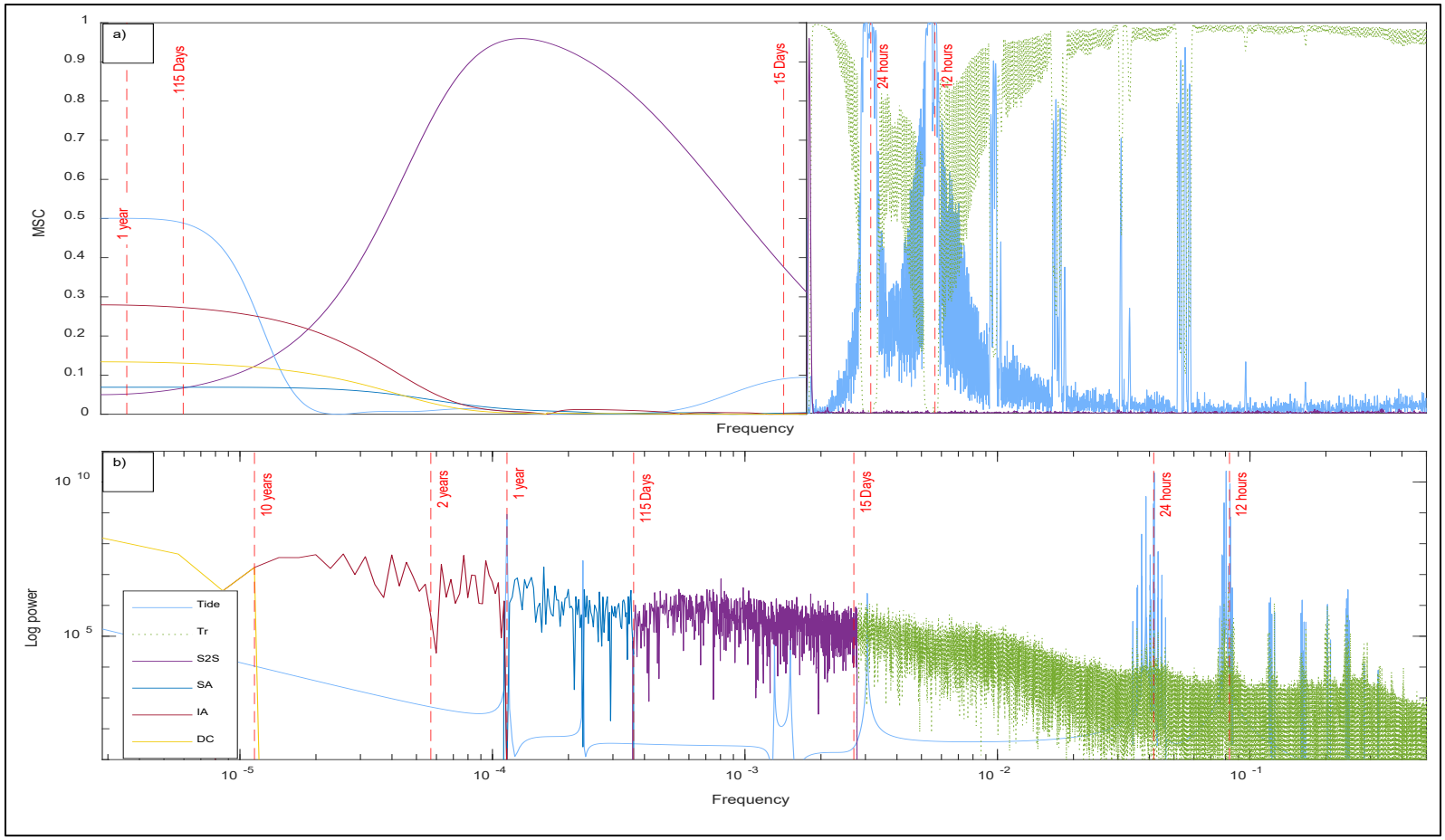

San Diego SWL a) magnitude-square coherence, and b) spectra calculated for findings assessment. Periodicity indicated (red dash lines).

Figure 29. San Diego SWL Spectra

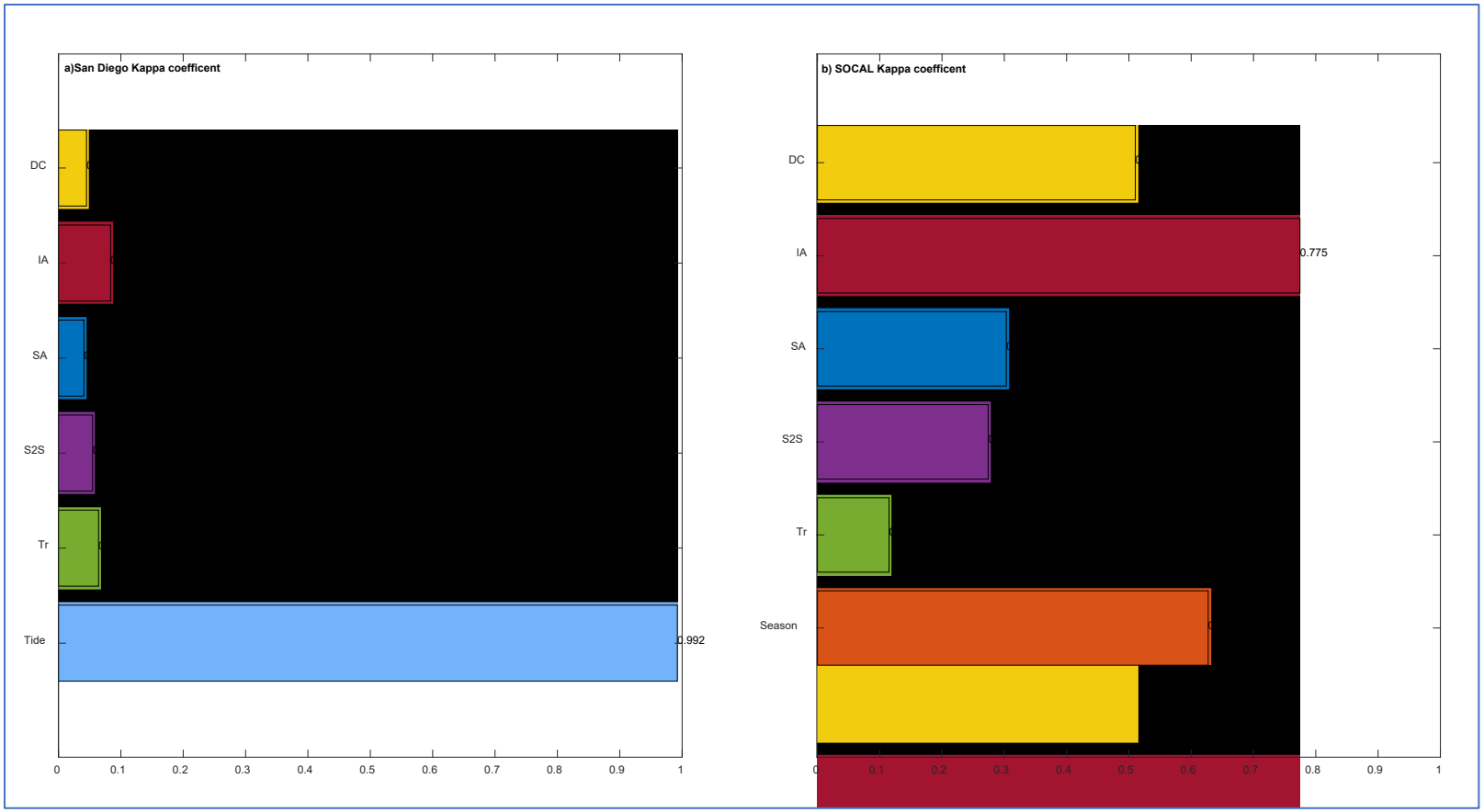

κ value of individual contributors for a) San Diego, and b) SOCAL.

Figure 30. San Diego κ Coefficients

THIS PAGE INTENTIONALLY LEFT BLANK

LIST OF REFERENCES

Alawad, K.A., Al-Subhi, A.M., Alsaafani, M.A., Alraddadi, T.M., Ionita, M., and Lohmann, G, 2019: Large-scale mode impacts on the sea level over the Red Sea and Gulf of Aden. *Remote Sensing*, **11**, 2224, https://doi:10.3390/rs11192224.

Amaya, D. J., M. G. Jacox, J. Dias, M. A. Alexander, K. B. Karnauskas, J. D. Scott, and M. Gehne, 2021: Subseasonal-to-seasonal forecast skill in the California Current System and its connection to coastal Kelvin waves. *Journal of Geophysical Research: Oceans*, e2021JC017892.

Arcodia, M. C., B. P. Kirtman, and L. S. P. Siqueira, 2020: How MJO teleconnections and ENSO interference impacts U.S. precipitation. *J. Climate*, **33**, 4621–4640, https://doi.org/10.1175/JCLI-D-19-0448.1.

Barnard, P.L., L.H. Erikson, A.C. Foxgrover, J.A.F. Hart, P. Limber, A.C. O'Neill, M. van Ormondt, S. Vitousek, N. Wood, M.K Hayden, and J.M. Jones, 2019: Dynamic flood modeling essential to assess the coastal impacts of climate change. *Scientific reports*, **9**, 4309, https://doi.org/10.1038/s41598-019-40742-z.

Beckley, B. D., P. S. Callahan, D. W. Hancock III, G. T. Mitchum, and R. D. Ray., 2017: On the "Cal-Mode" correction to TOPEX satellite altimetry and its effect on the global mean sea level time series. *Journal of Geophysical Research: Oceans*, **122**, 11, 8371–8384, https://doi.org/10.1002/2017JC013090.

Benveniste, J., F. Birol, F. Calafat, A. Cazenave, H. Dieng, Y. Gouzenes, J. F. Legeais et al., 2020: Coastal sea level anomalies and associated trends from Jason satellite altimetry over 2002–2018, *Scientific Data*, **7**, 357. 7. https://doi.org/10.1038/ s41597-020-00694-w.

Bindoff, N.L., J. Willebrand, V. Artale, A, Cazenave, J. Gregory, S. Gulev, K. Hanawa, C. Le Quéré, S. Levitus, Y. Nojiri, C.K. Shum, L.D. Talley and A. Unnikrishnan, 2007: Observations: oceanic climate change and sea level. In: *Climate change 2007: The physical science basis*. Contribution of working group I to the fourth assessment report of the intergovernmental panel on climate change [Solomon, S., D. Qin, M. Manning, Z. Chen, M. Marquis, K.B. Averyt, M. Tignor and H.L. Miller (eds.)]. Cambridge University Press, Cambridge, United Kingdom and New York, NY, USA.

Burks-Copes, K. A., Russo, E. J. J., Bourne, S., Case, M., Davis, A., Fischenich, C , M. Follum et al. 2014: *Risk quantification for sustaining coastal military installation assets and mission capabilities.* Army Corps of Engineers. Accessed April 30, 2021, http://www.dtic.mil/docs/citations/AD1039724.

Caldwell, P. C., M. A. Merrifield, P. R. Thompson, 2015: *Sea level measured by tide gauges from global oceans — The Joint Archive for sea level holdings* (NCEI Accession 0019568), Version 5.5, NOAA National Centers for Environmental Information, Dataset, doi:10.7289/V5V40S7W.

Carson, M., A. Köhl, D. Stammer, A. B. A. Slangen, C. A. Katsman, R. S. W. van de Wal, J. Church, and N. White, 2016: Coastal sea level changes, observed and projected during the 20th and 21st century. *Climatic Change*, **134**, 269–281, https://doi.org/10.1007/s10584-015-1520-1.

Cazenave, A. A., G. Le Cozannet, J. Benveniste, and P. L. Woodworth, 2017: Monitoring the change of coastal zones from space. Eos, *Transactions of the American geophysical union fall meeting abstracts*, OS13A-01, https://eos.org/opinions/monitoring-coastal-zone-changes-from-space.

Chadwick, B. et al., 2013: *A Methodology for Assessing the Impact of sea level rise on representative military installations in the southwestern United States* (RC-1703).

Chafik L, J. E. Ø. Nilsen, and S. Dangendorf, 2017: Impact of north Atlantic teleconnection patterns on northern European sea level. *Journal of Marine Science and Engineering*. **5, 3**, 43, https://doi.org/10.3390/jmse5030043.

Church, J. A., P. U. Clark, A. Cazenave, J. M. Gregory, S. Jevrejeva, A. Levermann, M. A. Merrifield et al. 2014: Sea level change. Climate change 2013: The physical science basis. Contribution of working group I to the fifth assessment report of the intergovernmental panel on climate change. Cambridge University Press, Cambridge, United Kingdom and New York, NY, USA, 1137–1216.

Codiga, D., 2022: UTide unified tidal analysis and prediction functions, accessed 02 January 2022, https://www.mathworks.com/matlabcentral/fileexchange/46523-utide-unified-tidal-analysis-and-prediction-functions.

Cui, M.; H.V. STORCH and E. Zorita, 1995: Coastal sea level and the large-scale climate state. A downscaling exercise for the Japanese islands. *Tellus A*, **47**, 132–144, https://doi.org/10.1034/j.1600-0870.1995.00008.x.

Dangendorf, S. et al., 2021: Data-driven reconstruction reveals large-scale ocean circulation control on coastal sea level. *Nature Climate Change*, **11, 6**, 514–520, https://doi.org/10.1038/s41558-021-01046-1.

Defense Science Board Washington, DC, 2011: Trends and implications of climate change for national and international security. Accessed October 30, 2021 https://apps.dtic.mil/sti/citations/ADA553407.

Ezer, T., 2013: Sea level rise, spatially uneven and temporally unsteady: Why the U.S. east coast, the global tide gauge record and the global altimeter data show different trends. *Geophysical Research Letters*. https://doi.org/10.1002/2013GL057952.

Felikson, D., G. A. Catania, T. C. Bartholomaus, M. Morlighem, and B. P.Y. Noël, 2020: Steep glacier bed knickpoints mitigate inland thinning in Greenland. *Geophysical Research Letters*, **48**, e2020GL090112. https://doi.org/10.1029/2020GL090112.

Fox-Kemper, B., H. T. Hewitt, C. Xiao, G. Aðalgeirsdóttir, S. S. Drijfhout, T. L. Edwards, N. R. Golledge, M. Hemer, R. E. Kopp, G. Krinner, A. Mix, D. Notz, S. Nowicki, I. S. Nurhati, L. Ruiz, J-B. Sallée, A. B. A. Slangen, Y. Yu, 2021, Ocean, cryosphere and sea level change. In: *Climate change 2021: The physical science basis. contribution of working group i to the sixth assessment report of the intergovernmental panel on climate change* [Masson-Delmotte, V., P. Zhai, A. Pirani, S. L. Connors, C. Péan, S. Berger, N. Caud, Y. Chen, L. Goldfarb, M. I. Gomis, M. Huang, K. Leitzell, E. Lonnoy, J. B. R. Matthews, T. K. Maycock, T. Waterfield, O. Yelekçi, R. Yu and B. Zhou (eds.)]. Cambridge University Press. In Press.

Frederikse, T., F. Landerer, F., L. Caron et al., 2020: The causes of sea-level rise since 1900. *Nature*, **584**, 393–397 (2020). https://doi.org/10.1038/s41586-020-2591-3.

Gharineiat, Z. and X.Deng, 2018: Description and assessment of regional sea-level trends and variability from altimetry and tide gauges at the northern Australian coast. *Advances in Space Research*, **61**, 10, 2540–2554. https://doi.org/10.1016/j.asr.2018.02.038.02.038.

Google Earth, Maps showing proof of concept area of study (Figure 1), accessed 28 December 2021.

Habel, S., C.H. Fletcher, T.R. Anderson et al. 2020: Sea-level rise induced multi-mechanism flooding and contribution to urban infrastructure failure. *Scientific reports*, **10**, 1–12. https://doi.org/10.1038/s41598-020-60762-4.

Hall J.A. et al., 2016: Regional sea level scenarios for coastal risk management: Managing the uncertainty of future sea level change and extreme water levels for department of defense coastal sites worldwide. Strategic Environmental Research And Development Program, Alexandria, VA, https://apps.dtic.mil/sti/citations/AD1013613.

Hamid, A. I. A., A. H. M. Din, C. Hwang, N. F. Khalid, A. Tugi, and K. M. Omar, 2018: Contemporary sea level rise rates around Malaysia: Altimeter data optimization for assessing coastal impact. *Journal of Asian Earth Sciences*, **166**, 247–259. https://doi.org/10.1016/j.jseaes.2018.07.034.

Hamlington, B. D., T. Frederikse, P.R. Thompson, J.K. Willis, R.S. Nerem and J.T. Fasullo, 2021: Past, present and future Pacific sea level-change. Earth's future, e2020EF001839. https://doi.org/10.1029/2020EF001839.

Hamlington, B. D., T. Frederikse, R.S. Nerem, J.T. Fasullo, and S. Adhikari, 2020: Investigating the acceleration of regional sea level rise during the satellite altimeter era. *Geophysical Research Letters*, **47**, https://doi.org/10.1029/2019gl086528.

Han W., G.A. Meehl, D. Stammer, A.X. Hu, B. Hamlington, J. Kenigson, H. Palanisamy and P. Thompson, 2017: *Spatial patterns of sea level variability associated with natural internal climate modes. Integrative study of the mean sea level and its components*. 221–254, https://doi.org/10.1007/978-3-319-56490-6_10.

Han, W., D. Stammer, P. Thompson et al., 2019: Impacts of basin-scale climate modes on coastal sea level: a review. *Surveys in geophysics*, **40**, 6 1493–1541. https://doi.org/10.1007/s10712-019-09562-8.

Hermans, T. H. J., Le Bars, D., Katsman, C. A., Camargo, C. M. L., Gerkema, T., Calafat, F. M. et al., 2020: Drivers of interannual sea level variability on the northwestern European shelf. *Journal of Geophysical Research: Oceans*, **125**, e2020JC016325. https://doi.org/10.1029/2020JC016325.

Huang, B., C. Liu, V. Banzon, E. Freeman, G. Graham, B. Hankins, T. Smith, and H.-M. Zhang, 2021: Improvements of the daily optimum interpolation sea surface temperature (DOISST) Version 2.1. *J. Climate*, **34**, 2923–2939, DOI 10.1175/JCLI-D-20-0166.1 (V2.1).

Idier, D., X. Bertin, X., P. Thompson et al., 2019: Interactions between mean sea level, tide, surge, waves and flooding: mechanisms and contributions to sea level variations at the coast. *Surveys in geophysics*, **40**, 1603–1630. https://doi.org/10.1007/s10712-019-09549-5.

IPCC, 2021: Climate Change 2021: The physical science basis. contribution of working group i to the sixth assessment report of the intergovernmental panel on climate change [Masson-Delmotte, V., P. Zhai, A. Pirani, S. L. Connors, C. Péan, S. Berger, N. Caud, Y. Chen, L. Goldfarb, M. I. Gomis, M. Huang, K. Leitzell, E. Lonnoy, J. B. R. Matthews, T. K. Maycock, T. Waterfield, O. Yelekçi, R. Yu and B. Zhou (eds.)]. Cambridge University Press. In Press.

Jiang, X., T. Li, and B. Wang, 2004: Structures and mechanisms of the northward propagating boreal summer intraseasonal oscillation. *Journal of Climate*, **17**, 1022–1039. https://doi.org/10.1175/1520-0442(2004)017<1022:SAMOTN>2.0.CO;2.

Kaplan D., 2004: Estimating significance level for coherences. School website. https://websites.pmc.ucsc.edu/~dmk/notes/cohere_signif/index.html.

Keogh, M. and T. Törnqvist, 2019: Measuring rates of present-day relative sea-level rise in low-elevation coastal zones: a critical evaluation. *Ocean Science*, **15**, 61–73. https://doi.org/10.5194/os-15-61-2019.

Kim, D.et al., 2009: Application of MJO simulation diagnostics to climate models. *Journal of Climate*, **22**,23, 6413–6436, https://doi.org/10.1175/2009JCLI3063.1.

Klotzbach, P. J., and E. C. J. Oliver, 2015: Modulation of Atlantic basin tropical cyclone activity by the Madden-Julian oscillation (MJO) from 1905 to 2011. *Journal of Climate*, **28**, 1, 204–217. https://doi.org/10.1175/JCLI-D-14-00509.1

Leamon, R. J., S.W. McIntosh, and D.R. Marsh, 2021: Termination of solar cycles and correlated tropospheric variability. *Earth and space science*, **8**, e2020EA001223. https://doi.org/10.1029/2020EA001223.

Liu, H., X. Feng, A. Tao, and W. Zhang, 2021: Intraseasonal variability of sea level in the western north Pacific. *Journal of Geophysical Research: Oceans*, **126**, e2021JC017237. https://doi.org/10.1029/2021JC017237.

Long, X. et al. 2021: Seasonal forecasting skill of sea-level anomalies in a multi-model prediction framework. *Journal of Geophysical Research: Oceans*, **126**, e2020JC017060. https:// doi.org/10.1029/2020JC017060.

Long, X., M. J. Widlansky, F. Schloesser, P. R. Thompson, H. Annamalai, M. A. Merrifield, and H. Yoon, 2020: Higher sea levels at Hawaii caused by strong El Niño and weak trade winds. *Journal of Climate*.**33**, 8, 3037–3059, https://doi.org/ 10.1175/JCLI-D-19-0221.1

Mantua, N.J. 1999: The Pacific decadal oscillation. A brief overview for non-specialists, *Encyclopedia of Environmental Change*.

Menéndez, M., and P. L. Woodworth, 2010: Changes in extreme high-water levels based on a quasi-global tide-gauge data set, *J. Geophys. Res.*, **115**, C10011, https://doi.org/10.1029/2009JC005997.

Merrifield M.A., A.S. Genz, C.P. Kontoes, J.J. Marra, 2013: Annual maximum water levels from tide gauges: contributing factors and geographic patterns. *J. Geophys Res.*, **118**, 2535–2546, https ://doi.org/10.1002/jgrc.2017.

Moss R. et al., 2016: Understanding data needs for vulnerability assessment and decision making to manage vulnerability of Department of Defense installations to climate change. Battelle Memorial Inst., Columbus, OH, https://apps.dtic.mil/sti/citations/ AD1025344.

NASA, 2000: Interplanetary Low Tide. Accessed 02 March 2022 https://science.nasa.gov/science-news/science-at-nasa/2000/ast04may_1m

National Centers for Environmental Prediction/National Weather Service/NOAA/U.S. Department of Commerce, 2005: updated monthly. Multiple Products, 1948-continuing. Research Data Archive at https://www.cpc.ncep.noaa.gov/products/precip/CWlink/MJO/climwx.shtml.

NAVFAC, 2017: *Navy climate change installation adaptation and resilience planning handbook*.

NAVFAC, 2020: Navy IGI&S sea level rise planning. southwest-GRC. 13.

Nerem, R., B. Beckley, B., J.Fasullo, B Hamlington, D. Masters, and G. Mitchum, 2018: Climate-change–driven accelerated sea-level rise detected in the altimeter era. Proceedings of the National Academy of Sciences, **115**, 2022–2025, https://doi.org/10.1073/pnas.1717312115.

Nidheesh, A. G., M. Lengaigne, J. Vialard, T. Izumo, A. S. Unnikrishnan, B. Meyssignac, B. Hamlington, and C. de Boyer Montégut , 2017: Robustness of observation-based decadal sea level variability in the Indo-Pacific ocean. *Geophysical Research Letters*, **44**, 7391–7400, https://doi.org/10.1002/2017GL073955.

NOAA National Weather Center, 2022: Climate prediction center, climate and weather linkage, last accessed 12 March 2022, https://tidesandcurrents.noaa.gov.

NOAA Tides and Currents, 2022: Center for operational oceanographic products and services water levels at multiple stations, last accessed 12 March 2022, https://tidesandcurrents.noaa.gov.

NOAA, 2021: Is sea level rising? National ocean service website, https://oceanservice.noaa.gov/facts/sealevel.html, 02/26/21.

Office of the Under Secretary of Defense for Acquisition and Sustainment, 2019: Report on the effects of a changing climate to the Department of Defense. Accessed September 21, 2021 https://media.defense.gov/2019/Jan/29/2002084200/-1/-1/1/climate-change-report-2019.PDF.

Oliver E.C.J., K.R. Thompson 2010: Madden-Julian Oscillation and sea level: Local and remote forcing. *J. Geophys Res.: Oceans*, **115**, C1, https://doi.org/10.1029/2009JC005337.

Oppenheimer, M., B.C. Glavovic , J. Hinkel, R. van de Wal, A.K. Magnan, A. Abd-Elgawad, R. Cai, M. Cifuentes-Jara, R.M. DeConto, T. Ghosh, J. Hay, F. Isla, B. Marzeion, B. Meyssignac, and Z. Sebesvari, 2019: Sea level rise and Implications for low-lying islands, coasts and communities. In: IPCC special report on the ocean and cryosphere in a changing climate [H.-O. Pörtner, D.C. Roberts, V. Masson-Delmotte, P. Zhai, M. Tignor, E. Poloczanska, K. Mintenbeck, A. Alegría, M. Nicolai, A. Okem, J. Petzold, B. Rama, N.M. Weyer (eds.)]. In press.

Ozbahceci, B., A.Turgut, A. Bozoklu, and S. Abdalla, 2020: Calibration and verification of century based wave climate data record along the turkish coasts using satellite altimeter data. *Advances in Space Research*, **66**, 10, 2319–2337. https://doi.org/10.1016/j.asr.2020.02.021.

Pajak, K. and K. Kowalczyk, 2018: A comparison of seasonal variations of sea level in the southern Baltic Sea from Altimetry and tide gauge data. *Advances in Space Research*, **63**, 5, 1768–1780. https://doi.org/10.1016/j.asr.2018.11.022.

Palmer, M. D. et al., 2020: Exploring the drivers of global and local sea-level change over the 21st century and beyond. *Earth's Future*, **8**, e2019EF001413. https://doi.org/10.1029/2019EF001413.

Parker, B.B, 2007: Tidal analysis and prediction. Silver Spring, MD, NOAA NOS Center for Operational Oceanographic Products and Services, 378 (NOAA Special Publication NOS CO-OPS 3). https://repository.oceanbestpractices.org/handle/11329/632.

Payo-Payo M.,and X. Bertin, 2020: The seasonal cycle of mean sea level in the north east Atlantic ocean. *J. Coast. Res.*, **95**, 1515–1519. https://doi.org/10.2112/SI95-292.1.

Piecuch, C. G., P. R. Thompson, R. M. Ponte, M. A. Merrifield, and B.D. Hamlington, 2019: What caused recent shifts in tropical Pacific decadal sea-level trends?. *Journal of Geophysical Research: Oceans*, **124**, 7575–7590. https://doi.org/10.1029/ 2019JC015339.

Prandi, P. et al. 2021: Local Sea level trends, accelerations and uncertainties over 1993–2019.*Sci Data*, **8**, 1 (2021). https://doi.org/10.1038/s41597-020-00786-7.

Pugh D.T. and P.L. Woodworth, 2014: *Sea-level science: Understanding tides, surges, tsunamis and mean sea- level changes*. Cambridge University Press, Cambridge.

Quartly, G.D., and A.A. Kurekin, 2020: Sensitivity of altimeter wave height assessment to data selection. *Remote Sensing*, **12**, 16, 2608. https://doi.org/10.3390/rs12162608.

Ray, R. D., and M.A. Merrifield, 2019: The semiannual and 4.4-yearmodulations of extreme high tides. *Journal of Geophysical Research: Oceans*, **124**, 5907–5922. https://doi.org/10.1029/2019JC015061.

Reynolds, Richard W., T. M. Smith, C. Liu, D. B. Chelton, K. S. Casey, and M. G. Schlax, 2007: Daily high-resolution-blended analyses for sea surface temperature. *J. Climate*, **20**, 5473–5496. https://doi.org/10.1175/2007JCLI1824.1.

Safi'i, A.N. and A.W. Rudiastuti, 2019: Tidal correlation using altimetry satellite. IOP Conference Series: Earth and Environmental Science. **284**, https://iopscience.iop.org/article/10.1088/1755-1315/284/1/012036/meta.

Schloesser, F., P. R. Thompson, and C.G. Piecuch, 2021: Meridional asymmetry in recent decadal sea-level trends in the subtropical Pacific Ocean. *Geophysical Research Letters*, **48**, e2020GL091959. https://doi. org/10.1029/2020GL091959.

Shumway, R. H., D. S.Stoffer, D. S. Stoffer, 2000: *Time series analysis and its applications*, Volume 3. New York: Springer.

Stammer, D., A. Cazenave, R.M. Ponte, M.E. Tamisiea, 2013: Causes for contemporary regional sea level changes. *Annual Review of Marine Science*, **5**, 21–46, https://doi.org/10.1146/annurev-marine-121211-172406.

Stockdon, H., R. Holman, P. Howd, A. Sallenger, 2006: Empirical parameterization of setup, swash, and runup. *Coastal Engineering*, **53**, 573–588. https://doi.org/ 10.1016/j.coastaleng.2005.12.005.

Tajfirooz, B., R. Arabsheibani and S. Behnia, 2018: GIS-based seamless tide prediction framework in the Persian Gulf. *Annals of GIS*, **24**, 2, 139–150, https://doi:10.1080/19475683.2018.1424733.

Thompson, D.W.J., and J.M. Wallace, 2000: Annular modes in the extratropical circulation. Part I: Month-to-month variability. *J. Climate*, **13**, 1000–1016, https://doi.org/10.1175/1520-0442(2000)013<1000:AMITEC>2.0.CO;2.

Thompson, P. R., M. J. Widlansky, B. D. Hamlington, M. A. Merrifield, J. J. Marra, G. T. Mitchum, and W. Sweet, 2021: Rapid increases and extreme months in projections of United States high-tide flooding. *Nature Climate Change*, **11**, 7, 584–590, https://doi.org/10.1038/s41558-021-01077-8

Trenberth, K., and National Center for Atmospheric Research Staff, 2020: The climate data guide: Nino SST Indices (Nino 1+2, 3, 3.4, 4; ONI and TNI). Accessed 06 May 2021 https://climatedataguide.ucar.edu/climate-data/nino-sst-indices-nino-12-3-34-4-oni-and-tni.

Tseng, K.C., E. Maloney, and E.A. Barnes, 2020: The consistency of MJO teleconnection patterns on interannual time scales. *Journal of Climate*, **33**, 9, 3471–3486. https://doi.org/10.1175/JCLI-D-19-0510.1

U.S. Congress. Government Accountability Office, 2017: Climate change adaptation: DOD needs to better incorporate adaptation into planning and collaboration at overseas installations. *Congressional Publications*. Accessed 14 May 2020 https://www.gao.gov/assets/gao-18-206.pdf.

U.S. Congress. Government Accountability Office, 2019: Climate resilience: DOD needs to assess risk and provide guidance on Use of climate projections in installation master plans and facilities designs. *Congressional Publications*. Accessed 30 June 2020 https://www.gao.gov/assets/gao-19-453.pdf.

U.S. Department of Defense. *Office of the Under Secretary of Defense for acquisition and sustainment, 2019: Report on the effects of a changing climate to the Department of Defense*. Accessed 10 January 2020 https://media.defense.gov/2019/Jan/29/2002084200/-1/-1/1/climate-change-report-2019.PDF.

Unnikrishnan, A.S., A. Matthews, M. Gravelle, L. Testut, T. Aarup, P. L. Woodworth, and B. A. Kumar, 2019: Tide gauges. 31–34: Beal, L. M.; J. Vialard, M.K. Roxy, 2019: IndOOS-2: A roadmap to sustained observations of the Indian Ocean for 2020–2030. CLIVAR/IOC-GOOS *Indian Ocean Region Panel (IORP)*, 31–34. https://doi:10.36071/clivar.rp.4.2019.

Vandervort, J., 2020: Sea level rise and beyond: Is the U.S. military prepared for climate change?. *Bulletin of the Atomic Scientists*, **76**, 3, 145–149, https://doi:10.1080/00963402.2020.1751971.

Wang G., L. Cheng, T. Boyer, C. Li, 2017: Halosteric sea level changes during the Argo era. *Water*, **9**, 7, 484. https://doi.org/10.3390/w9070484.

Welch, P. D., 1967: The use of the fast fourier transform for the estimation of power spectra: A method based on time averaging over short, modified periodograms. *IEEE Transactions on Audio and Electroacoustics*, **15**, 70–73. https://doi:10.1109/TAU.1967.1161901.

Woodworth, P. L., G. Wöppelmann, M. Marcos, M. Gravelle, and R. M. Bingley, 2017b: Why we must tie satellite positioning to tide gauge data. Eos *Trans Am Geophys Union*, **98**, 4, 13–15. https ://doi.org/10.1029/2017e o0640 37, https ://eos.org/opini ons/why-we-must-tie-satel lite-posit ionin g-totide-gauge -data

Woodworth, P.L., A. Melet, M. Marcos, R.D. Ray, G. Wöppelmann, Y.N. Sasaki, M. Cirano, A. Hibbert, J.M. Huthnance, S. Monserrat, and M.A. Merrifield, 2019: Forcing factors affecting sea level changes at the coast. *Surveys in Geophys*, **40**, 1351–1397, https://doi.org/10.1007/s10712-019-09531-1.

World Meteorological Organization, 2021: KNMI Climate explorer daily climate indices. Accessed 03 October 2021, https://climexp.knmi.nl/selectdailyindex.cgi?id=someone@somewhere

Wright D. J., C. Harder, 2021: GIS for science: Maps for saving the planet, Volume 3, ECU. https://doi.org/10.17128/9781589485877.

Xu, Q., K. Tu, Y. Cheng, W. Wang, Y. Jia, and X. Ye, 2019: Satellite altimetry and tide gauge observed teleconnections between long-term sea level variability in the U.S. East Coast and the north Atlantic Ocean. *Remote Sensing*, **11**, 23, 2816, https://doi.org/10.3390/rs11232816.

Zhu, Y., G. T. Mitchum, P.R. Thompson, and G.S.E. Lagerloef, 2021: Diagnosis of large-scale, low-frequency sea level variability in the northeast Pacific ocean. *Journal of Geophysical Research: Oceans*, **126**, e2020JC016682. https://doi.org/10.1029/2020JC016682

Zlotnicki, V.; Z. Qu, W. Joshua, 2019: MEaSUREs gridded sea surface height anomalies version 1812. PO.DAAC, CA, USA, accessed 12 October 2020, https://doi.org/10.5067/SLREF-CDRV2.

INITIAL DISTRIBUTION LIST

1. Defense Technical Information Center
   Ft. Belvoir, Virginia

2. Dudley Knox Library
   Naval Postgraduate School
   Monterey, California